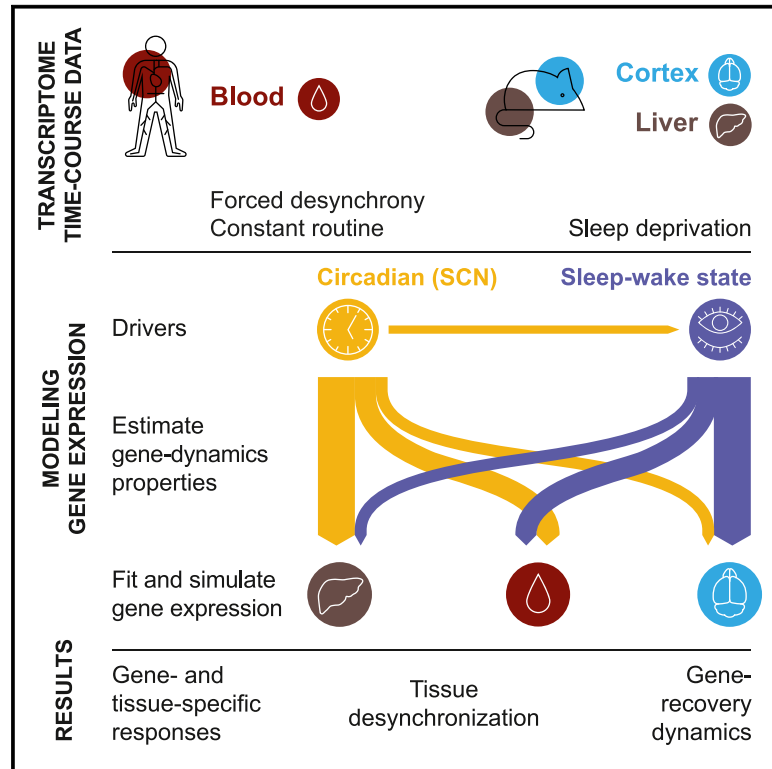


# Cell Systems

## Model integration of circadian- and sleep-wake-driven contributions to rhythmic gene expression reveals distinct regulatory principles

### Graphical abstract



### Authors

Maxime Jan, Sonia Jimenez, Charlotte N. Hor, Derk-Jan Dijk, Anne C. Skeldon, Paul Franken

### Correspondence

maxime.jan@unil.ch (M.J.), paul.franken@unil.ch (P.F.)

### In brief

Circadian- and sleep-wake-dependent contributions to the daily changes in gene expression are difficult to disentangle. Using a mathematical model, we evaluated the relative circadian and sleep-wake contributions in time course transcriptome data. The model showed that genes and tissues have distinct sensitivities, which explained the divergent molecular responses to sleep perturbations.

### Highlights

- A driven, damped harmonic oscillator explains complex daily transcriptome rhythms
- Sleep-wake drive can lead to delayed and long-term responses in gene expression
- Clock-gene expression in cerebral cortex is more sleep-wake driven than circadian
- Mistimed waking and sleep desynchronize transcription within and across tissues



Article

# Model integration of circadian- and sleep-wake-driven contributions to rhythmic gene expression reveals distinct regulatory principles

Maxime Jan,<sup>1,2,\*</sup> Sonia Jimenez,<sup>1</sup> Charlotte N. Hor,<sup>1</sup> Derk-Jan Dijk,<sup>3,4</sup> Anne C. Skeldon,<sup>4,5</sup> and Paul Franken<sup>1,6,\*</sup>

<sup>1</sup>Center of Integrative Genomics, University of Lausanne, Lausanne, Switzerland

<sup>2</sup>Bioinformatics Competence Center, University of Lausanne, Lausanne, Switzerland

<sup>3</sup>Surrey Sleep Research Centre, University of Surrey, Guildford, UK

<sup>4</sup>Care Research & Technology Centre, UK Dementia Research Institute, Imperial College London and University of Surrey, Guildford, UK

<sup>5</sup>School of Mathematics and Physics, University of Surrey, Guildford, UK

<sup>6</sup>Lead contact

\*Correspondence: [maxime.jan@unil.ch](mailto:maxime.jan@unil.ch) (M.J.), [paul.franken@unil.ch](mailto:paul.franken@unil.ch) (P.F.)

<https://doi.org/10.1016/j.cels.2024.06.005>

## SUMMARY

Analyses of gene-expression dynamics in research on circadian rhythms and sleep homeostasis often describe these two processes using separate models. Rhythmically expressed genes are, however, likely to be influenced by both processes. We implemented a driven, damped harmonic oscillator model to estimate the contribution of circadian- and sleep-wake-driven influences on gene expression. The model reliably captured a wide range of dynamics in cortex, liver, and blood transcriptomes taken from mice and humans under various experimental conditions. Sleep-wake-driven factors outweighed circadian factors in driving gene expression in the cortex, whereas the opposite was observed in the liver and blood. Because of tissue- and gene-specific responses, sleep deprivation led to a long-lasting intra- and inter-tissue desynchronization. The model showed that recovery sleep contributed to these long-lasting changes. The results demonstrate that the analyses of the daily rhythms in gene expression must take the complex interactions between circadian and sleep-wake influences into account. A record of this paper's transparent peer review process is included in the supplemental information.

## INTRODUCTION

Throughout the brain and body, many transcripts exhibit 24 h rhythms.<sup>1–3</sup> These transcriptome rhythms are thought to emerge from cell-autonomous oscillations generated by clock genes engaged in negative transcriptional/translational feedback loops (TTFLs).<sup>4</sup> The circadian TTFL results in rhythmic expression not only of the clock genes themselves but also that of the numerous other genes they target, many of which are transcription factors, thereby setting off daily recurring cascades of transcriptional events comprising the rhythmic transcriptome. Within and among tissues, phase coherence is maintained by systemic cues originating from by the central circadian clock, which in mammals is located in the suprachiasmatic nuclei (SCN) of the hypothalamus, thereby acting as an internal zeitgeber entraining brain and body TTFLs.<sup>5,6</sup> Transcriptome data have contributed to our current understanding of the molecular architecture of the circadian clock and its tissue-specific functions.<sup>7,8</sup>

Transcriptome studies have also been used in sleep research, in particular to uncover genes and gene pathways implicated in the processes related to the sleep-wake-driven changes in sleep pressure. Studies in rats and mice showed

that sleep-wake states alter the brain transcriptome.<sup>9–12</sup> Among the affected transcripts, changes in many activity-induced immediately early genes (IEGs) reliably followed the time course of sleep-wake prevalence both during undisturbed baseline conditions and during sleep deprivation (SD).<sup>13,14</sup> Their sleep-wake-driven dynamics could be modeled using exponential saturating functions with time constants similar to those describing the dynamics of delta power,<sup>14</sup> a widely used electroencephalogram (EEG)-derived measure gauging sleep pressure. Examples of such transcripts are *Arc* and *Homer1a*, which both play a role in homeostatic down-scaling of synapses, a process considered as one of sleep's major functions.<sup>15–18</sup> Interestingly, we found that the brain expression of the core clock-genes *Npas2* and *Clock* followed dynamics similar to that of the sleep-wake-driven IEGs and that rhythm amplitudes of all but one of the other clock genes showed a long-term reduction in rhythm amplitudes following a single, short SD.<sup>14</sup> Combined with other observations, this suggests a considerable molecular crosstalk between circadian- and sleep-wake-driven processes in the brain.<sup>19,20</sup>

Since under undisturbed conditions the sleep-wake distribution is circadian and because sleep-wake behavior drives the



expression of numerous transcripts, many of the genes found to be rhythmic in circadian transcriptome studies might oscillate as a consequence of the daily changes in the prevalence of sleep-wake states and not as a direct consequence of the circadian TTFLs. We and others found that when the time-spent-awake prior to tissue sampling was controlled, the majority of rhythmically expressed genes in the cortex (73%–81%) no longer oscillate.<sup>15,21</sup> Similarly, scheduling sleep in anti-phase with the time it normally occurs in a forced desynchrony (FD) protocol flattened the rhythm of the blood transcriptome in humans, including that of several clock genes.<sup>22</sup> These observations show that sleep-wake-driven factors contribute to the rhythmic changes in gene expression in brain and body tissues peripheral to the SCN.

Determining which genes and pathways are rhythmic as a result of changes in sleep-wake behavior or due to circadian systemic cues, is of importance when, e.g., assessing the factors underlying the long-term health consequences of circadian misalignment that have been attributed mainly to circadian factors.<sup>23,24</sup> In an earlier effort, we categorized transcripts as either sleep-wake driven or circadian driven using the concepts of the two-process model of sleep regulation,<sup>14</sup> a model that stipulates that sleep is regulated by a circadian process (process C) of sinusoidal shape that interacts with a sleep-wake-driven process (process S) modeled after the dynamics of EEG delta power.<sup>25</sup> In that study,<sup>14</sup> we analyzed cortical samples taken under baseline conditions and during and after a 6 h SD. The results confirmed that most (63%) of the cortical transcripts that were rhythmic under undisturbed baseline conditions were categorized as sleep-wake driven when considering the entire time course. It is, however, unlikely that the rhythmic expression of a given gene is influenced only by either one of the two processes. Moreover, this approach required model selection among a set of models with different number of free parameters, which is not without issues, and only one type of sleep-wake-driven dynamic (i.e., “process S” type) was considered. Finally, the marked long-term consequences of SD on expression dynamics we discovered in that study, especially that of most clock genes, could not be captured by any of the models unless circadian amplitude after the SD was altered in the model.

Here we implement a driven, damped harmonic oscillator model to estimate the separate contributions of sleep-wake and circadian processes to the rhythmic transcriptome. In this model, circadian systemic cues and sleep-wake-driven influences are considered simultaneously as driving factors that effectively accelerate or decelerate oscillations in gene expression. By changing the damping ratio, the model can capture both the dynamics of intrinsically oscillating transcripts (i.e., underdamped in the model) and of overdamped transcripts for which the sleep-wake response approximate exponential saturating functions of process S. We applied the model to transcriptome data obtained in mouse cortex and liver tissue and in human blood and successfully captured the wide range of transcription dynamics observed under conditions of SD, FD, and a constant routine (CR) following 7 days of sleep restriction.<sup>14,22,26</sup> The results give new insights into the complex interaction between circadian- and sleep-wake-driven influences on gene expression.

## RESULTS

### Datasets used to disentangle circadian- and sleep-wake-dependent influences

Under undisturbed, entrained conditions, sleep-wake dependent and circadian contributions to rhythmic gene expression cannot be separated as both factors fluctuate in synchrony with stable phase relationships. To quantify their respective contributions, the timing of sleep (and wakefulness) relative to circadian phase needs to be altered experimentally. In the first dataset used for the current analyses, gene expression in cortex and liver was quantified in mice at 18 time points before (baseline), during, and after (recovery) a 6 h SD (Figure 1A). Sleep-wake behavior was recorded in a separate cohort of mice undergoing the same experimental protocol. The SD kept mice awake at a time-of-day animals are normally mostly asleep, i.e., the first half of the light period (zeitgeber time [ZT] 0–ZT6). The sleep-wake data and cortical transcriptomes were taken from our publicly available data,<sup>12,14,27</sup> while we acquired liver RNA sequencing data taken from the same mice to assess tissue specificity of gene-expression dynamics. A second dataset, also publicly available, consists of 2 experiments quantifying the blood transcriptome in humans using microarrays.<sup>22,26</sup> In the first experiment, participants completed a FD protocol in which a 28 h sleep-wake cycle was imposed, causing the circadian rhythm to “free-run” at its intrinsic, close-to-24 h period. Blood was sampled at 4 h intervals during a 28 h day when sleep was scheduled at the circadian phase at which it normally occurs during entrained conditions (“in-phase”) and during a 28 h day when sleep occurred in anti-phase with the circadian cycle (“anti-phase”; Figure 1B). In the second experiment, participants were given sleep opportunities of either 10 (“control sleep”) or 6 h (“restricted sleep”) during which they obtained 8.5 and 5.7 h of sleep, respectively, for 7 consecutive days preceding a CR during which participants were kept awake for ~40 h with blood samples taken every 3 h (Figure 1C). During the CR, light conditions, activity, and food intake were strictly controlled. Before the FD and CR experiments, sleep was recorded at habitual bedtime (“baseline”; 7.5 h of sleep), which we used as the sleep-wake distribution under “steady-state” conditions. Although the FD and CR experiments affected the timing and duration of sleep-wake behavior, circadian phase, assessed by blood melatonin and cortisol rhythms, remained remarkably unperturbed.<sup>22,28</sup> This is consistent with analyses of clock-gene rhythms in the mouse SCN, which indicated that the central circadian pacemaker is not much affected by changes in the sleep-wake distribution,<sup>29–32</sup> although SD has been shown to reduce neuronal activity within the SCN.<sup>33</sup> Furthermore, SD does not alter the phase of circadian activity patterns in mice.<sup>34</sup>

Rhythmic gene expression can follow a dynamic that could be regarded as strictly sleep-wake driven or as strictly circadian driven, illustrated by *Homer1* expression in cortex and *Bmal1* expression in liver, respectively. *Homer1* expression decreases during the light phase when mice are mostly asleep, increases during the dark when mice are mostly awake, further increases during SD, and quickly re-assumes baseline dynamics during recovery (Figure 1D), with little circadian influence.<sup>15</sup> By contrast, liver *Bmal1* expression oscillates throughout the

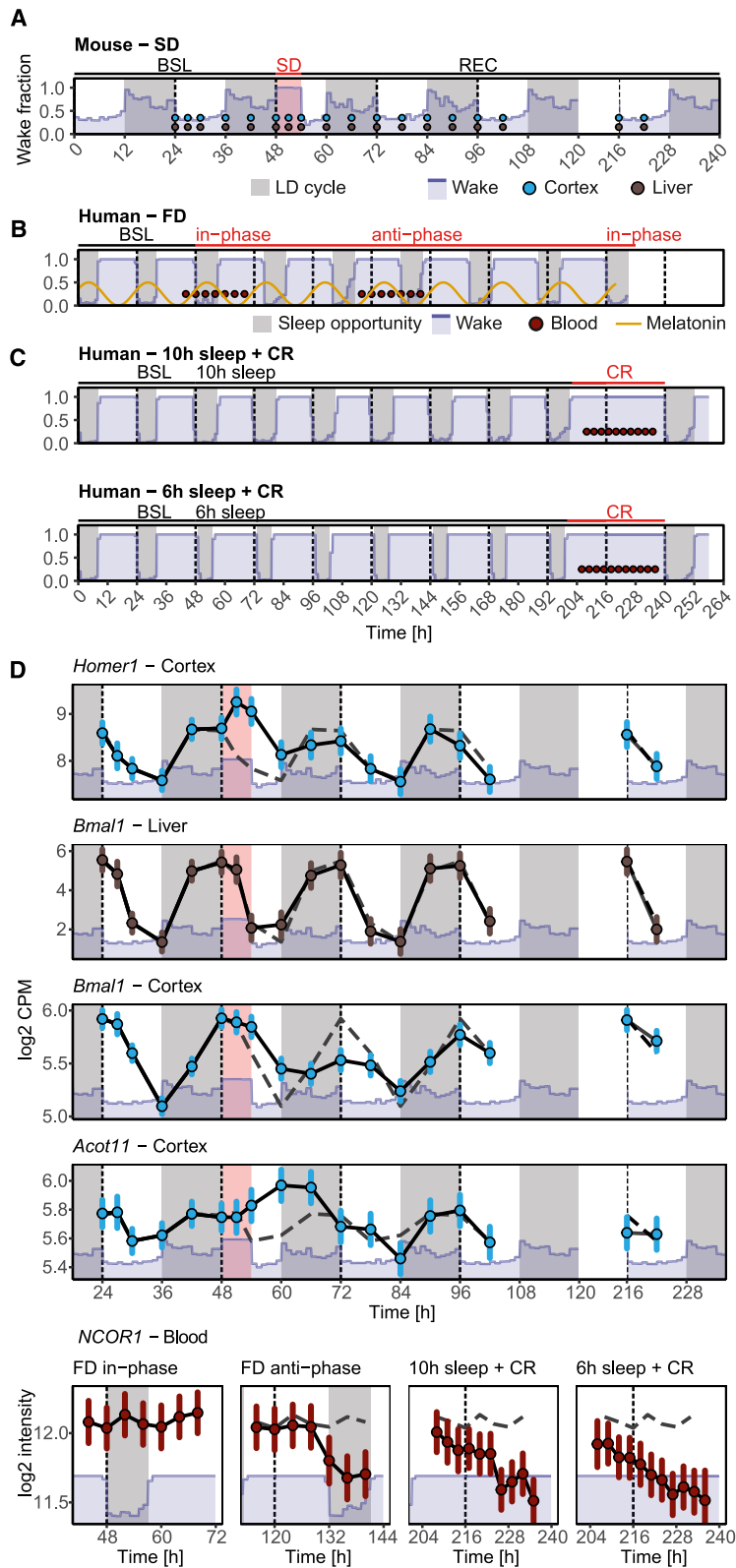


**Figure 1. Sleep-wake experiments in mice and humans**

(A) Sleep deprivation (SD) in mice. Mean fraction of time-spent-awake per hour of recording time (blue line/area,  $n = 12$ ) during baseline (BSL; days 1 and 2), 6 h SD (pink square starting at  $t = 48$  on day 3) and recovery (days 3–5 and 10). A 2<sup>nd</sup> batch of mice was used for tissue sampling of cortex (blue) and liver (brown points;  $n = 62$ ). Gray background represents the dark periods of the 12:12 h light-dark cycle. Note that the last 2 samples were taken 7 days after the SD.

(B) Forced desynchrony (FD) in humans. Mean wake fraction (blue area,  $n = 32$ ) during the 28 h sleep-wake cycles of the FD. Blood samples (red points) were taken during a 28 h day when participants slept in-phase and during a 28 h day when sleep occurred in anti-phase with their circadian melatonin profile. Gray boxes represent scheduled sleep opportunities.

(C) Constant routine (CR) experiments in humans. Mean wake fraction (blue area,  $n = 36$ ) after a 7-day control (top: “10 h sleep”) and a restricted (bottom: “6 h sleep”) sleep-opportunity schedule. Blood samples (red points) were taken during the CRs.

(D) Examples of gene expression dynamics in cortex (blue), liver (brown), and blood (red symbols) with mean gene expression (95% CI; mice:  $n = 3$ –5 per time point; human: 8–24 per time point). Solid black lines connect time points, and dashed gray lines replicate baseline in mice (before SD) or in-phase dynamics in humans. Details as in (A)–(C).

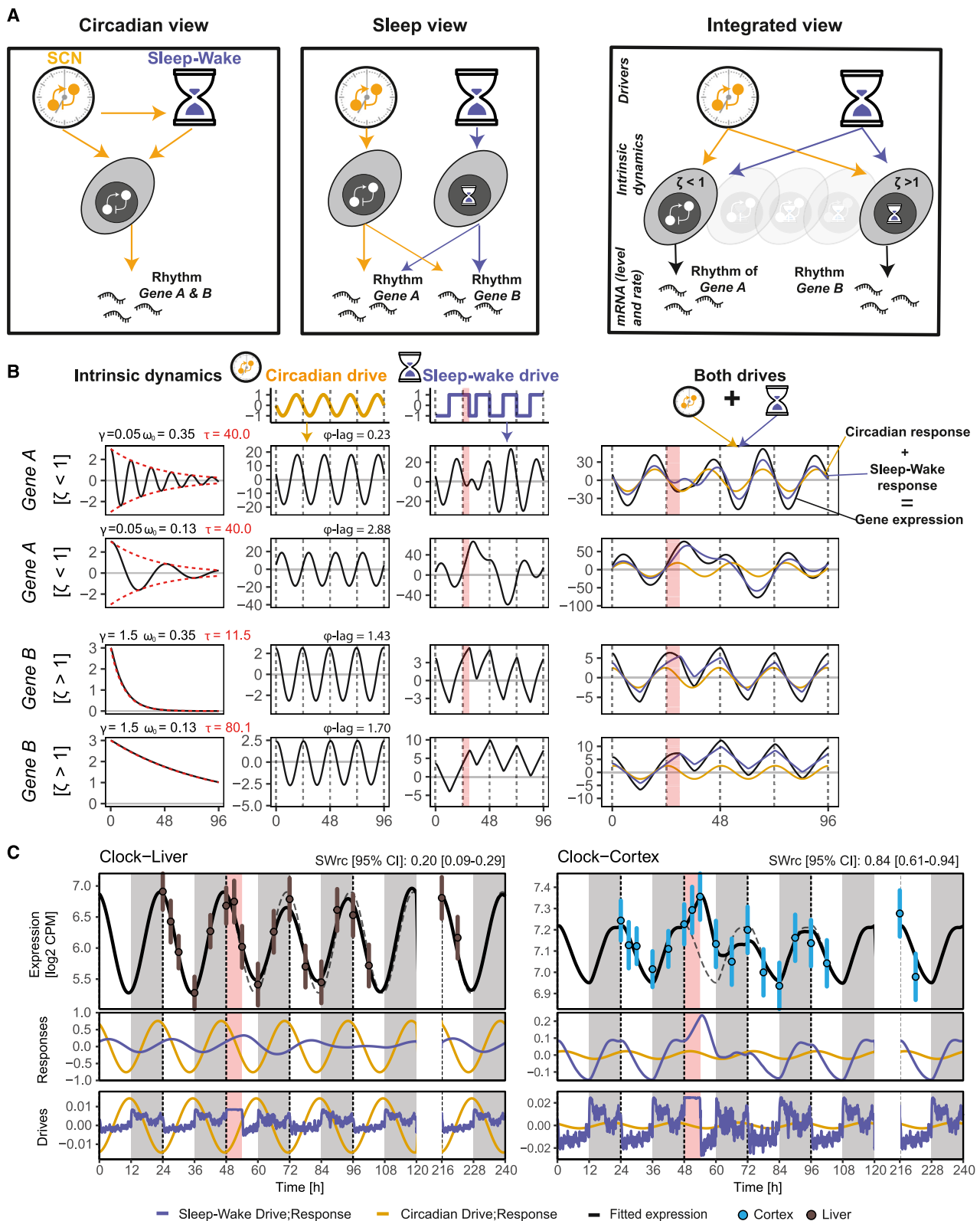


**Figure 2. Modeling gene expression using a damped-driven harmonic oscillator**

(A) Schematic of the circadian view of rhythmic gene expression (left) in which the SCN directly or indirectly drive or entrain oscillations of gene expression generated by local circadian clocks (TTFL) in peripheral cells. The sleep view (middle) separates circadian- and sleep-wake-related genes, each regulated by

(legend continued on next page)

experiment largely unperturbed by SD (Figure 1D), consistent with *Bmal1* being a core circadian clock gene.<sup>35</sup> Rhythmically expressed genes can, however, show dynamics that do not follow such simple rules.<sup>14</sup> For example, while we find that during baseline the time course of cortical and liver expression of *Bmal1* is similar, SD leads to a long-lasting reduction in rhythm amplitude during recovery in the cortex but not in the liver (Figure 1D). This amplitude reduction outlasts the effects of SD on recovery sleep,<sup>14</sup> indicating that cortical *Bmal1* expression does not seem to simply follow the sleep-wake distribution. Another example is *Acot11*, a gene encoding an enzyme involved in the homeostatic regulation of free fatty-acids<sup>36</sup> and of non-rapid eye movement (NREM) sleep duration.<sup>12</sup> *Acot11* expression in the cortex increases with SD, and its baseline time course seems consistent with that of a sleep-wake-driven gene as it decreases during the light and increases during the dark when animals are predominantly asleep and awake, respectively. Yet, subsequent to SD, this relationship appears to invert, as sleep during initial recovery (ZT6–ZT12) is now associated with a strong increase in *Acot11* expression, leading to sustained high levels during the recovery dark phase (Figure 1D). A last example is the dynamics of nuclear corepressor 1 (*NCOR1*) expression, which encodes a protein affecting the clock-gene circuitry by acting as co-repressor to the clock-gene *REVERB $\alpha$*  (*NR1D1*) and by activating HDAC3.<sup>37–39</sup> During the FD, blood *NCOR1* expression appears rhythmic only when sleep occurs in anti-phase with the circadian rhythm (Figure 1D), which might suggest that under normal, in-phase conditions, the sleep-dependent decrease in *NCOR1* expression is opposed by a circadian-dependent increase. However, such a scenario cannot easily explain the downregulation of *NCOR1* expression with extended wakefulness observed during the two CRs in the second experiment (Figure 1D).

These examples illustrate that rhythmic gene expression results from an often complex interaction between the responses to circadian- and sleep-wake-dependent drives that seem to greatly differ among genes and tissues. Quantifying and comparing the relative importance of these factors in driving the rhythmic transcriptome requires a modeling approach that can integrate sleep-wake- and circadian-dependent influences on gene expression.

### Rhythmic gene expression as a driven, damped harmonic oscillator

Transcriptome rhythms measured in peripheral organs are thought to arise from TTFLs made up of the core circadian clock

genes.<sup>4</sup> According to this scenario, local tissue rhythms are kept in phase with each other and with the light-dark cycle by signals generated by the SCN. At the same time, the SCN drive rhythms in overt behaviors such as sleep and wakefulness (Figure 2A, left).<sup>40,41</sup> Although perturbations of sleep are known to impact gene expression, most studies only examined the immediate effects of SD, and only a few considered the influence of the sleep-wake distribution on the rhythmic transcriptome.<sup>9,14,22,26</sup> Similarly, modeling sleep-wake-driven dynamics using exponential saturating functions, following the example of the dynamics of EEG delta power,<sup>14,42</sup> does not include a circadian component, and interactions between circadian and sleep-wake-related factors, beyond simple additive effects, have not been considered (Figure 2A, middle). The model we propose allows for such interaction and provides a framework to quantify the relative contribution of circadian- and sleep-wake-dependent factors on rhythmically expressed genes. These genes can be modeled as intrinsically rhythmic, i.e., because they are closely associated with the circadian TTFL, or they can appear rhythmic because they follow circadian- and/or sleep-wake-dependent drives but, in the absence of such recurring drives, do not oscillate (Figure 2A, right). We have used earlier implementations of this modeling approach to simulate the effects of sleep-wake state on *Per2* mRNA and protein levels.<sup>43,44</sup>

The measured level of the expression of a gene reflects the net result of mRNA synthesis and degradation. With our data, we cannot assess whether changes in gene expression resulted from changes in synthesis, degradation, or both. We nevertheless use these terms when referring to a net increase and decrease in mRNA levels. We propose a framework in which the level of mRNA of a gene is  $X(t)$  where  $t$  is time. We suppose that the rate of synthesis of  $X(t)$  will depend on intra-tissue factors such as the levels and activity of transcription factors, temperature, and metabolites affecting mRNA regulation, which we group together in a single “tissue environment” variable  $Y(t)$ . We suppose the rate of degradation depends on the level of  $X(t)$ . In the simplest (linear) approximation, the rate of change of mRNA may be written as

$$\frac{dX}{dt} = \alpha Y - \gamma X \quad (\text{Equation 1})$$

where  $\alpha$  describes the effect of the tissue environment on the synthesis rate of  $X(t)$  and  $\gamma$  is the degradation rate per unit  $X(t)$ . We assume that the tissue environment variable is affected by external factors  $F(t)$  such as the circadian and sleep-wake drives

different dynamics. The integrated view (right) considers each gene to be regulated to a varying degree by systemic circadian- and sleep-wake-dependent influences, which act as drives on gene expression in the periphery.

(B) Illustration of the damped-driven harmonic oscillator model. According to a gene’s intrinsic properties, two types of expression dynamics can be observed when expression is removed from equilibrium and no drive is applied: an underdamped system oscillating with a decaying amplitude (upper, hypothetical *Gene A*, damping ratio  $\zeta < 1$ ) and an overdamped system (bottom, *Gene B*,  $\zeta > 1$ ) where expression returns to equilibrium position without oscillation according to exponential decaying function (red dashed lines) with a time-constant  $\tau$  determining the time it takes to recover. For each gene, examples of two  $\omega_0$  values are given: 0.35 and 0.13 (rad/h), illustrated in the upper and lower row panels, respectively. External recurring driving factors are required to maintain gene expression entrained and rhythmic (circadian drive in yellow, sleep-wake drive in purple; middle two panels). The difference between  $\omega_0$  and the frequency of the external drive determines the phase-lag ( $\phi$ -lag) between drive and response. Combining the responses to each drive generates the observed rhythm in gene expression (right). Pink areas represent sleep deprivation.

(C) Model fit for expression of *Clock* in liver (left) and cortex (right). Circadian (yellow) and sleep-wake (purple) drives applied on the model (bottom), circadian and sleep-wake responses to the drives giving the best fit (middle), fitted expression in black with mean gene expression (95% CI,  $n = 3\text{--}5/\text{time point}$ ; upper). Dashed gray lines replicate baseline. *SWrc* (with 95% CI) is the relative contribution of the sleep-wake response (see results).

and that there is feedback between the gene of interest and the tissue environment so that

$$\frac{dY}{dt} = -\beta X + F(t) \quad (\text{Equation 2})$$

where  $\beta$  describes the strength of the feedback between the gene of interest and the tissue environment.

We let  $X(t) = X_b + x(t)$ ,  $Y(t) = Y_b + y(t)$ , and  $F(t) = F_b + f(t)$ , where  $X_b$ ,  $Y_b$ , and  $F_b$  are fixed baseline values that satisfy Equations 1 and 2 when  $\frac{dX}{dt} = \frac{dY}{dt} = 0$ . Then substituting for  $X(t)$  and  $Y(t)$  in Equations 1 and 2, differentiating (Equation 1) with respect to time and substituting in for  $\frac{dY}{dt}$  from Equation 2) leads to the equation for a damped harmonic oscillator (Equation 3; see STAR Methods).

$$\frac{d^2x}{dt^2} + \gamma \frac{dx}{dt} + \omega_0^2 x = f(t) \quad (\text{Equation 3})$$

where  $\omega_0^2 = \alpha\beta$  and  $f(t) = \alpha f(t)$ . In this equation,  $x(t)$  represents the level of mRNA of a gene quantified as normalized counts from RNA sequencing (in  $\log_2$  counts per million, or CPM) for the mouse tissues or from Affymetrix microarrays (in  $\log_2$  probe intensities) for human blood samples. The term  $\omega_0^2 x$  arises from the feedback between the gene and its environment and could be viewed as, e.g., an auto-inhibition through negative feedback,<sup>45</sup> as is the case for the expression of clock genes that comprise the circadian TTFL. A large value of  $\omega_0^2$  translates into a strong negative feedback controlling gene expression. By contrast, a weak negative feedback will result in gene expression rhythms being driven mostly by changes in external factors. Another intrinsic factor determining gene expression dynamics is the degradation constant,  $\gamma$ , which opposes changes in gene expression and introduces a time delay in response to external driving factors.

The model can capture both intrinsically oscillatory and non-oscillatory genes. Using the standard terminology of simple harmonic oscillators in the absence of time dependent external driving factors ( $f(t) = 0$ ), when the damping ratio,  $\zeta = \gamma / 2\omega_0 < 1$ , the oscillator is said to be underdamped. When released from a position away from equilibrium, the expression of the hypothetical gene, *Gene A*, will oscillate around equilibrium with an amplitude that decreases on a timescale determined by damping constant  $\gamma$  (Figure 2B, top two rows). However, when  $\zeta > 1$  (i.e., overdamped), gene expression will not oscillate and reverts to the equilibrium directly (hypothetical *Gene B*; Figure 2B, bottom two rows). For underdamped genes, the time required for the expression to return to equilibrium ( $\tau$ ) is determined by  $\gamma$ , while for overdamped genes it depends on  $\gamma$  and  $\omega_0$  (Equation 4; Figure 2B, red line).

$$\text{Time constant } [\tau] \text{ to equilibrium} \approx \begin{cases} -\frac{1}{-\frac{\gamma}{2} + \sqrt{\left(\frac{\gamma}{2}\right)^2 - \omega_0^2}}, & \zeta > 1 \\ 2/\gamma, \zeta & < 1 \end{cases} \quad (\text{Equation 4})$$

Recurring external driving factors ( $f(t)$  in Equation 3) are needed to assure phase coherence of the daily transcriptome changes among and within tissues and, if  $\gamma > 0$ , to maintain

rhythmicity. Such external factors can either follow continuous oscillations (Figure 2B, 2<sup>nd</sup> column) originating, for example, from the SCN or result from discrete physiological or behavioral events such as being (kept) awake or asleep (Figure 2B, 3<sup>rd</sup> column), which in this schematic includes an SD (pink bars). We refer to these two types of driving factors as “circadian-driven factor” ( $f_C(t)$ ) and “sleep-wake-driven factor” ( $f_{SW}(t)$ ), respectively. In the model, we base  $f_{SW}$  on the fraction of sleep ( $S(t)$ ; i.e., NREM + rapid eye movement [REM] sleep) and wakefulness ( $W(t)$ ), measured within a given time interval,  $t$ , multiplied by their respective coefficients,  $\beta_s$  and  $\beta_w$  (Equation 5; see STAR Methods). The circadian drive,  $f_C(t)$ , is modeled as a sinewave with a 24 h period and a free phase and amplitude ( $\varphi$  and  $A$ ; Equation 5).

$$\begin{aligned} f_{SW}(t) &= \beta_w W(t) + \beta_s S(t) \\ f_C(t) &= A \sin\left(\frac{2\pi}{24}t + \varphi\right) \end{aligned} \quad (\text{Equation 5})$$

Together, these two factors affect the rhythmic expression of a gene by increasing or decreasing its acceleration, i.e., the rate of change of its synthesis rate.

The combined effect of the two driving factors on the oscillator can be mathematically decomposed into the responses to either factor (see STAR Methods). Summing the separate contributions again reconstructs the gene-expression dynamics fitted by the model (Figure 2B, right column). In the Figure 2B schematic, the relative contributions of the two driving factors (and their respective responses) to the expression dynamics of *Genes A* and *B* are similar in magnitude prior to SD, yet because of their different intrinsic properties, the response to the same sleep-wake perturbation can differ. Besides  $\zeta$ , the response also depends on the phase-lag between the oscillator and the drive, which is determined by the frequency ratio ( $r = \omega/\omega_0$ ) between the frequency of the drive ( $\omega = \frac{2\pi}{24}$ ) and the natural frequency ( $\omega_0$ ) (Equation 3). If  $r = 1$ , the phase-lag is  $\frac{\pi}{2}$ , and the oscillator is said to be in resonance. If  $r \gg 1$ , the phase-lag increases and an inertia in the response of the oscillator is observed such that the rate of gene expression will only slowly change after a change in the external drive. By contrast, when  $r \ll 1$ , the phase-lag decreases, causing the rate of gene expression to change already before the external driving factors can exert their influence because of the feedback generated by the system.

$$\varphi - \text{lag} = \begin{cases} \arctan\left(\frac{2\zeta r}{1-r^2}\right) + \pi, & r < 1 \\ \arctan\left(\frac{2\zeta r}{1-r^2}\right), & r \geq 1 \end{cases} \quad (\text{Equation 6})$$

With different contributions from the two external driving factors and different intrinsic parameters, the model can capture a large variety of dynamics (Figure 2B, right column).

The parameters  $\gamma$ ,  $\omega_0$ ,  $\beta_w$ ,  $\beta_s$ ,  $A$ , and  $\varphi$  of the model were estimated by fitting gene expression in mouse cortex, liver, and human blood (STAR Methods). The parameters, together with their 95% confidence intervals (CIs), were estimated independently for each gene and tissue (Table S1). Figure 2C illustrates the responses to the two driving factors the model estimated for the expression dynamics of *Clock* with different results in the two

tissues. As for *Bmal1* (Figure 1D), *Clock* expression in the liver displays a sinewave oscillation unperturbed by SD. By contrast, cortical *Clock* expression decreased when animals were asleep, increased when awake spontaneously and during SD (Figure 2C). Although the model fitted the *Clock* expression dynamics equally well in the two tissues (Kendall's  $\tau = 0.56$  and  $0.73$  in cortex and liver, respectively), the damping ratio greatly differed ( $\zeta = 0.79$  and  $0.06$ , respectively). In liver,  $f_C$  and its response was much stronger than that of  $f_{SW}$ , while the opposite was observed in the cortex where *Clock* dynamics resembled that of a sleep-wake-driven gene such as *Homer1* (Figure 1B).<sup>14</sup> We quantified the relative contribution of the two drives by calculating a sleep-wake response contribution (*SWrc*) metric as follows: the peak-to-trough amplitude of the response to  $f_{SW}$  ( $A_{SWr}$ ) in baseline was expressed as a fraction of the peak-to-trough amplitude of the summed response to the 2 drives ( $A_{SWr} + A_{Cr}$ ; Equation 7). *SWrc* can vary between 0 and 1 with 0 indicating that the summed response is entirely due to  $f_C$ , 1 to  $f_{SW}$ , and 0.5 indicating equal contributions.

$$\text{sleep-wake response contribution (SWrc)} = \frac{A_{SWr}}{A_{SWr} + A_{Cr}} \quad (\text{Equation 7})$$

For the expression of *Clock*, *SWrc* in liver was 0.20 and in cortex 0.84 (Figure 2C), reflecting well the circadian- and sleep-wake-driven nature of the dynamics in the two respective tissues, comparable to *SWrc* values obtained for *Bmal1* expression in liver (0.10) and *Homer1* in cortex (0.83; Figure 3).

Our model not only reliably captured straightforward gene expression dynamics but also less predictable scenarios. A “pure” sleep-wake-driven gene will tightly follow the sleep-wake distribution, independent of circadian phase, and the gene will be intrinsically strongly damped, together resulting in dynamics approximating those following exponential functions such as observed for many IEGs,<sup>14</sup> including *Homer1* (Figure 3), and for EEG delta power (Figure S1). On the other hand, the expression of a pure circadian-driven gene will continue oscillating because it is intrinsically underdamped and responds only to circadian drives (i.e., a low *SWrc*) such that amplitude and phase are unaffected by changes in sleep-wake state as was observed for *Bmal1* and *Clock* in liver (Figures 2C and 3). For the 3 remaining genes highlighted in Figure 1 the sleep-wake and circadian drives contributed approximately equally to their expression dynamics (*SWrc*: 0.49–0.69; Figure 3; Table S2). Yet, because of their different intrinsic properties (Table S2), expression dynamics responded very differently to the drives applied. Although wakefulness accelerated cortical *Bmal1* expression, its expression did not increase during SD because (1) the natural frequency ( $\omega_0 = 0.2$ ; Table S2) was close to the baseline sleep-wake frequency (0.26, i.e., 24 h;  $\approx$  resonance), and thus the sleep-wake response was already close to *Bmal1*'s maximum amplitude, and (2) the circadian response decreased during the SD. The prolonged amplitude reduction of *Bmal1*'s oscillation after SD resulted from a combination of a low damping constant (Table S2), which increased the time to return to equilibrium ( $\tau = 20$  h, Equation 4), and the reduction in time-spent-awake during the recovery dark period, which reduced the normal increase in gene expression rate at

this time of day. Wakefulness also accelerated the rate of cortical *Acot11* expression (Figure 3). The peculiar, prolonged increase in *Acot11* during recovery sleep was due to a weak negative feedback ( $\omega_0^2$ ) and thus a long phase-lag between drive and response (Table S2). This inertia of the SD-accumulated wake drive was strong as it would have required 2 h of continuous sleep to counter it. In addition to this inertia, the interaction between the circadian and sleep-wake responses kept expression elevated for 9 h after SD, further delaying a reduction of *Acot11* expression. Wakefulness decelerated the rate of *NCOR1* expression in human blood, and the continued decrease in *NCOR1* expression during the CRs was modeled by weak negative feedback. Modeling *NCOR1* expression dynamics further highlighted that the contribution of the sleep-wake response relative to that of the circadian response depends on the experimental condition: in baseline the two contributions were similar (*SWrc* = 0.69; Table S2), but in anti-phase, thereby flattening *NCOR1*'s expression, while during the CRs, when subjects are kept awake for 40 h, the sleep-wake contribution became the dominant drive (*SWrc* = 0.90).

These examples underscore that a gene's expression can appear rhythmic for a variety of reasons, which can differ according to tissue. Moreover, the circadian- and sleep-wake-driven influences on the expression of some genes can be revealed only during longer-term sleep disruptions and would have gone unnoticed under undisturbed conditions. Our strategy differs (and captures other genes) from simply assessing differential expression immediately after the SD, which has been used to categorize a gene as sleep-wake driven (Figure S2).

### Assessing the model's performance against alternative models

We evaluated the performance of the model and possible overfitting by comparing it to both simpler and more complex models, considering all datasets. The evaluation was performed on the subset of genes and probe sets that showed rhythmic expression during baseline for mice and when sleep occurred in phase with melatonin production for humans. As mentioned earlier, pure sleep-wake-driven and pure circadian-driven genes can display undistinguishable rhythmic patterns in baseline. Both categories of genes can thus be captured in an unbiased fashion with a simple sinewave fit and independently of their response to sleep perturbation. The time courses of the top 1,000 most significant “sinusoidal” genes per tissue (cortex, liver, and blood) were used to assess the model's performance, i.e., a total of 3,000 genes.

Our model has 6 free parameters ( $k = 6$  [ $\gamma, \omega_0, \beta_s, \beta_w, \phi, A$ ]; see Equations 3 and 5), with the equilibrium position (intercept) fixed to the mean gene expression in baseline in mouse and in-phase data in human. The model integrated the two human transcriptome experiments as one, and model parameters were simultaneously optimized. We did, however, allow different intercepts between the FD and the CRs after the control- and restricted-sleep conditions ( $k = 7$ ).

To evaluate the fit and complexity of our model (hypothesis 1 or  $H_1$ ), we contrasted it to the following 4 alternative models ( $H_A$ ; for details, see STAR Methods): (1) a linear regression model based on independent fixed effects for each time point ( $k = 18$  and 35 in mouse and human, respectively) known to over-fit

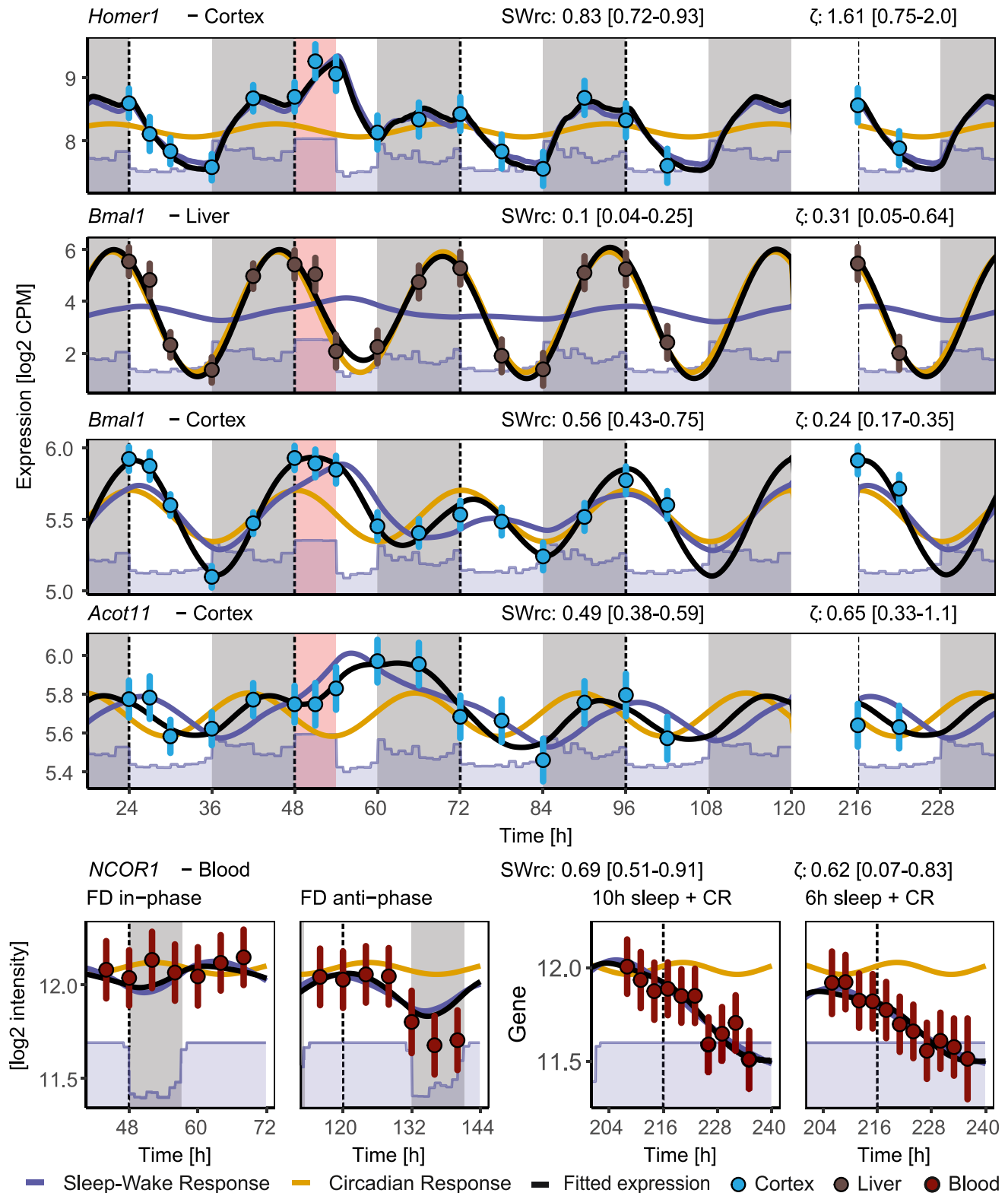


**Figure 3. Model fits for the genes illustrated in Figure 1D**

Fitted dynamics (black line) with mean expression and 95% CI of cortical *Homer1* expression follows almost exclusively the sleep-wake response (purple line), while *Bmal1* in the liver the circadian response (yellow line). *Bmal1* and *Acot11* in cortex and *NCOR1* in blood follow a combination of a sleep-wake and circadian response. Details as in Figure 1D.

the data,<sup>14</sup> (2) the oscillator model with a sleep-wake drive only or, (3) with a circadian drive only ( $k = 4$  and  $5$ ), and (4) a simple additive model in which a fixed circadian effect (sinewave) is added to a sleep-wake effect without intrinsic dynamics integrating these effects ( $k = 5$  and  $6$ ). We compared the Bayesian information criterion (BIC) statistic of each of the 4  $H_A$  models to that of  $H_1$ . In general, the  $\Delta\text{BIC}$  indicated more genes with a better fit for  $H_1$  over both simpler and more complex models ( $\Delta\text{BIC} > 0$ : 97%, 61%, 88%, and 68% of all 3,000 genes, for  $H_A$  i-iv, respectively), even when using a more stringent cutoff ( $\Delta\text{BIC} > 2$ : 97%, 55%, 85%, and 63%, respectively; Figure S3A, top). In some cases,  $\Delta\text{BIC}$  favored  $H_A$ , although a strong support was found only for a minority of genes or probes ( $\Delta\text{BIC} < -2$ : 2%, 30%, 7%, and 24%, respectively). It shows that despite having far fewer parameters than the linear model with independent time effect, goodness of fit for  $H_1$  is still high ( $\sim 0.1$   $\Delta\text{Kendall's } \tau$ ) and is improved compared with simpler models (Figure S3A, bottom). This analysis supports  $H_1$  as it improved the overall fit, while model complexity did not increase too much over simpler models.

### The cortical transcriptome is mainly sleep-wake driven, and that of the liver and blood is mainly circadian driven

We then applied the  $H_1$  model to the entire transcriptome to detect, in an unbiased manner, any gene that would be sleep-wake driven and/or circadian driven by contrasting the results to a flat model with a single intercept as null hypothesis ( $H_0$ ) where expression variance represents noise. With a  $\Delta\text{BIC} > 2$  as rejection threshold, the model classified a large number of genes as rhythmically expressed: 7,237 (42% of 17,185) and 5,770 (43% of 13,373) genes in cortex and liver, respectively, and 18,548 probes (45% of 41,162) in blood (Figure S3B). Mean goodness of fit for rhythmic genes was high in mouse cortex and liver (Kendall's  $\tau$ :  $\sim 0.5$ ; Figure S3B, right) but somewhat lower for the human blood dataset both for all probes and the 1,000 rhythmic probes ( $\Delta$  mean Kendall's  $\tau$  for all probes: 0.17; for the 1,000 rhythmic probes: 0.12) but nevertheless still close to that of the more complex model (Figure S3A).

To assess and visualize the main source of variance for these rhythmically expressed genes, we performed a principal-component analysis (PCA; Figures 4 and S4; see STAR Methods) and projected the model fits in PCA space together with the corresponding circadian- and sleep-wake-driven responses plotted alongside the PC axes to show their respective contributions for the time segments depicted in the PC plots (Figures 4A–D). In addition, the complete simulated time course of the responses to  $f_{SW}$  and  $f_C$  for the first two principal components, PC1 and PC2, is illustrated underneath each panel for each of the experiments.

In the mouse cortex, PC1 displayed a predominant sleep-wake-driven response (projected  $SWrc = 0.80$ ) typical of IEGs. PC2 was determined by genes responding to both circadian and sleep-wake drives ( $SWrc = 0.60$ ) with the latter drive increasing gene expression during SD, which continued during the first 6 h of recovery (i.e., until ZT12 of the first recovery day; ZT12<sub>REC</sub> in Figure 4A), although mice were mostly asleep during this period. Such inertia to the sleep-wake response is similar to that described above for the dynamics of *Acot11* expression (Figure 3).

In the mouse liver, the fitted trajectories for the expression of genes contributing to PC1 and PC2 followed circular patterns with a large contribution of the circadian response ( $SWrc = 0.18$  and  $0.29$ , respectively), albeit with different phases (Figures 4B and S4, liver). SD decreased PC2 (T54<sub>ZT6</sub>), which was followed by a reduction in rhythm amplitude 12 h later (T66<sub>ZT18</sub>). This highlights, like for PC2 in the cortex, a slower type of sleep-wake-driven response requiring more time to change mRNA levels compared with the fast IEG (and EEG delta-power) -like responses that characterize the genes contributing to PC1 in cortex.

For the human blood transcriptome, PCA of the FD in-phase and anti-phase conditions (Figure 4C) shows that PC1's overall amplitude reduced during the anti-phase condition as sleep-wake and circadian responses became opposed to each other (Figure 4C, bottom). PC2 was mostly sleep-wake driven ( $SWrc = 0.78$ ), and because of the longer sleep and wake periods of the 28 h day (compared with the 24 h day), the amplitudes of the rhythmic probes contributing to this PC gradually increased to a new steady state after the initial 4 days of the FD protocol (Figure 4C, bottom).

PCA for the CR transcriptome experiment showed that the large effect of the 40 h wakefulness during the two CRs amplified the sleep-wake response ( $SWrc$ ) contributing to PC2 (from 0.56 in baseline to 0.70 during the CR), as was already illustrated for *NCOR1* (Figure 3). The preceding 7 days of restricted sleep changed the initial condition of the CR compared with that of the control condition (6 vs. 10 h sleep opportunity), again affecting mostly PC2, the trajectory of which was downshifted during the CR (Figure 4D, left vs. right upper).

As the PCA reports only on those transcripts contributing most to the overall variance, we assessed the  $SWrc$  values for the complete rhythmic transcriptome (Figure 5, on the diagonal). As already indicated by its PC1, the model found that cortical gene transcription was more sleep-wake driven than that of liver and blood, with similar  $SWrc$  values obtained in the latter two tissues (mean  $SWrc$ : 0.62, 0.37, and 0.40 for cortex, liver, and blood, respectively). In cortex, 67% of rhythmic genes were underdamped ( $\zeta < 1$ ), while 85% and 89% of genes in liver and blood were underdamped. Of all genes found to be rhythmic across the datasets (14,435;  $\Delta\text{BIC}_{10} > 2$ ), only 10% (1,468) were rhythmic in all 3 tissues. This small overlap of rhythmic genes was already observed in the pairwise tissue comparisons (21%, 27%, and 30% in the cortex-liver, cortex-blood, and liver-blood comparisons, respectively; Figure 5, above the diagonal). Tissue specificity of rhythmic genes has been noted before in other species.<sup>46</sup> We then compared the  $SWrc$  of the shared rhythmic genes ( $\Delta\text{BIC}_{10} > 2$ ). Genes rhythmic in the cortex were found to be predominantly more sleep-wake driven than in liver (826 out of 840 with non-overlapping 95% CI) and blood (762/826), and in blood more sleep-wake driven than in liver (335/436) (Figure 5, below the diagonal; Table S1). Among the rhythmic genes that were more sleep-wake driven in cortex than in liver most clock genes could be found (Table S1; see Figure 6A). We did not find any correlations for  $SWrc$  values between tissues (Pearson correlations; cortex vs. liver: 0.08, cortex vs. blood:  $-0.001$ , liver vs. blood: 0.003), indicating that the cause of rhythmicity (circadian vs. sleep-wake driven) was not shared.

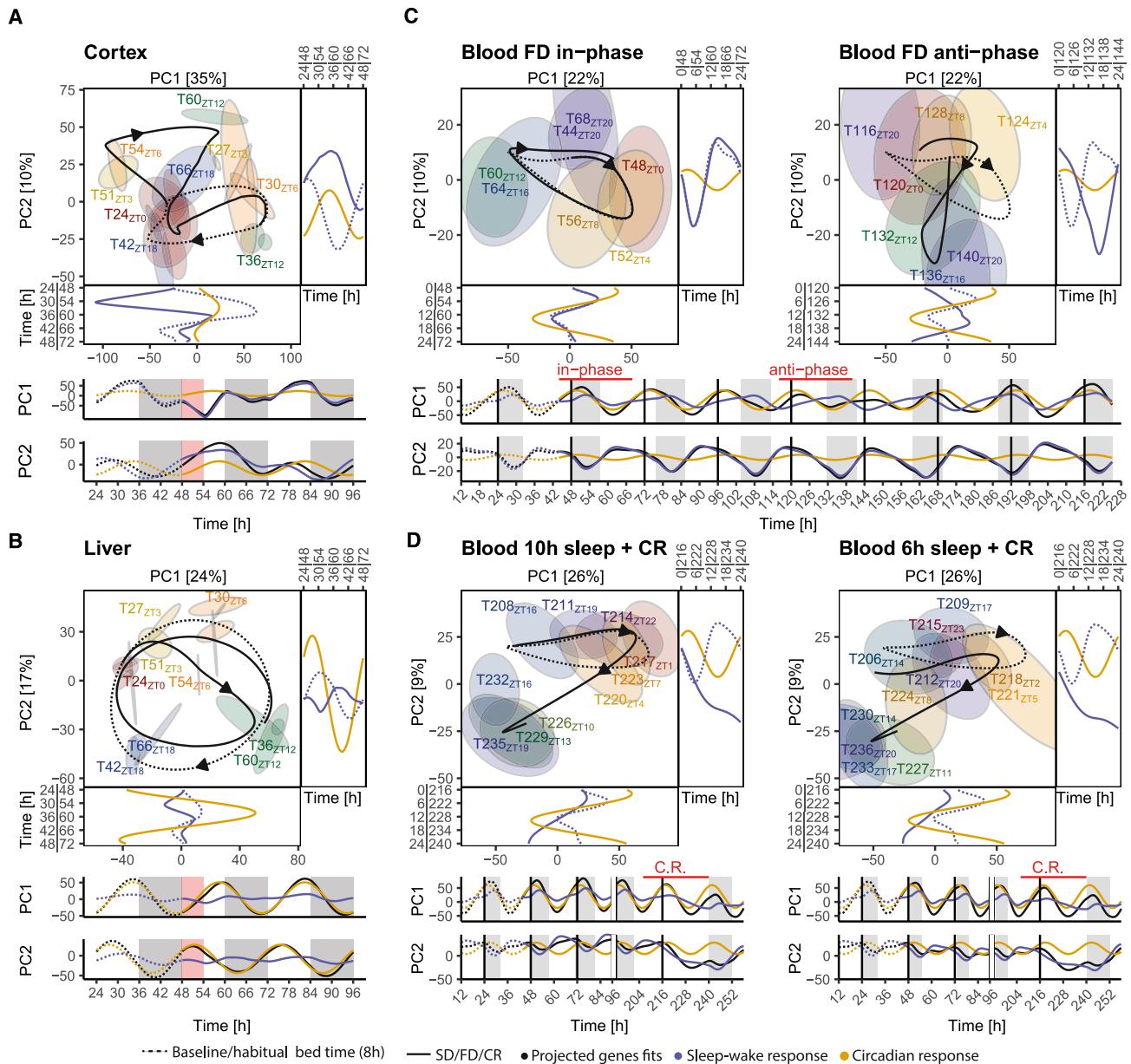


**Figure 4. PCA of the rhythmic transcriptomes**

(A) PCA in the mouse cortex (7,237 genes) and (B) liver (5,770 genes) during baseline (BSL), sleep deprivation (SD), and recovery (REC), (C) in human blood (18,548 probes) during the forced desynchrony (FD) when sleeping in-phase (left) and anti-phase (right), and (D) in human blood during the constant routine (CR) after the 10 h sleep (left) and 6 h sleep opportunity (right). Variance explained by each PC in brackets. Projected model fits in PCA space during BSL and habitual bedtime as dashed lines, fitted expression during SD + REC, FD, and CR conditions as solid lines. Arrowheads point to the progression in time. Ellipses delimit 95% CI of data acquired at each time point. Corresponding circadian (yellow) and sleep-wake (purple line)-driven responses are plotted alongside the PC axes. Note double labels at time axes corresponding to the respective times in the experiment for the two conditions (see time courses below). The complete simulated time course of the circadian- and sleep-wake-driven responses for PC1 and PC2 is illustrated underneath each panel for each of the experiments. Pink and gray boxes indicate the SD and dark periods, respectively, in mice, gray boxes for human experiments the scheduled sleep episodes.

### SD desynchronizes the tissue transcriptome

Although central and tissue rhythms in gene expression are generally associated with clock genes implicated in the TTFL, clock genes did not feature among the top circadian-driven genes. We therefore took a closer look at the expression dynamics of 15 core clock genes (Figure 6A). In the cortex, expression of 9/15 clock genes showed a significantly higher sleep-

wake-driven response than in the liver, with *Clock* having the strongest sleep-wake drive ( $SWrc = 0.84$ ). The  $SWrc$  values for clock genes in blood were often intermediate between those obtained in cortex and liver. Because the  $SWrc$  values for most clock genes differed between cortex and liver, sleep perturbation may alter inter-tissue synchrony and clock-gene-related processes like metabolism.<sup>47</sup> To assess tissue differences in

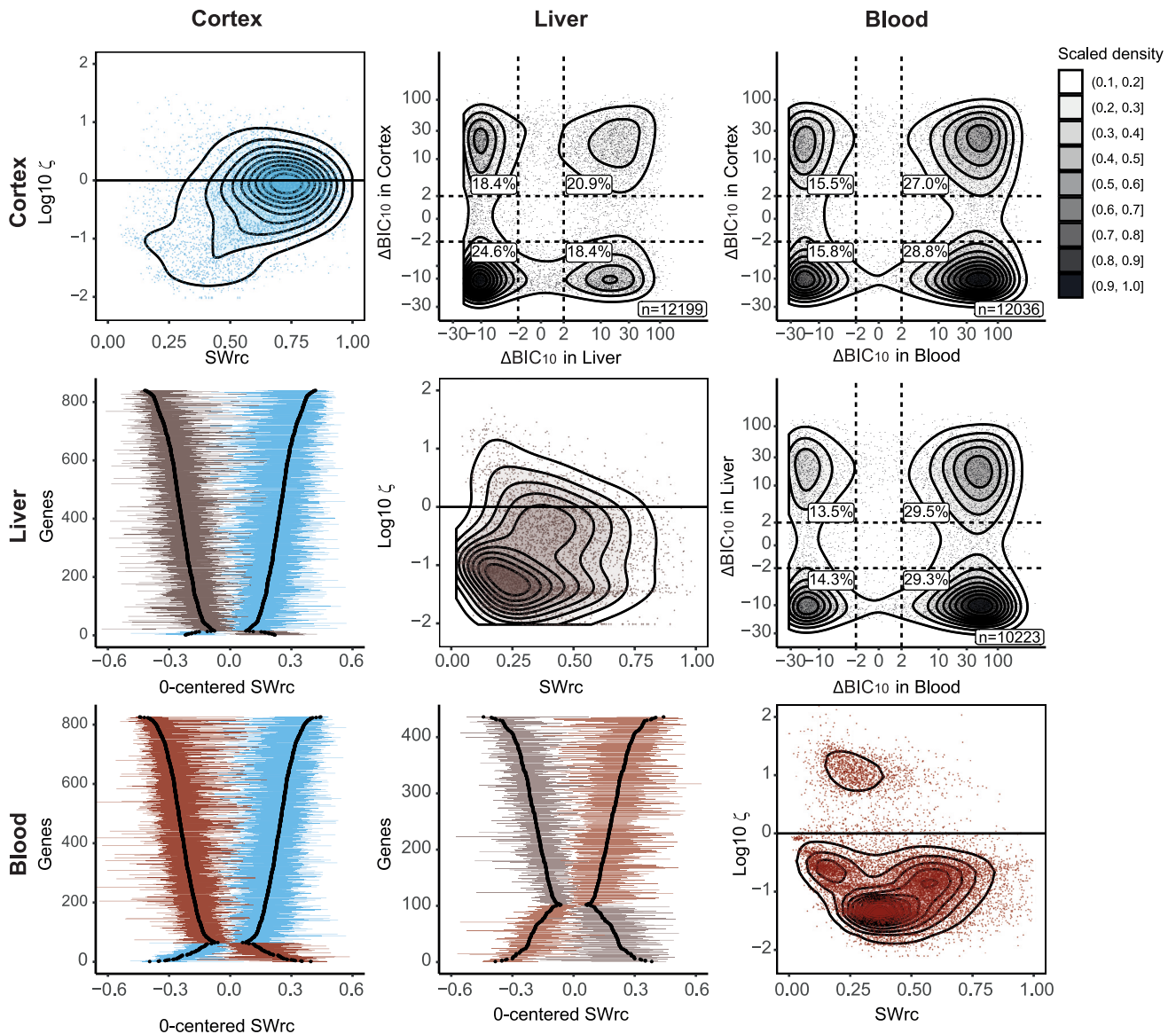


**Figure 5. Comparison of model parameters between tissues**

On the diagonal: relative sleep-wake response contribution ( $\text{SWrc}$ ) vs. damping ratio ( $\zeta$ ) for all rhythmic genes in cortex (blue, top,  $n = 7,237$ ), liver (brown, middle;  $n = 5,770$ ), and blood (red dots, bottom;  $n = 18,548$ ). Black lines represent 2D gene density. Above the diagonal: comparison of rhythmic genes between tissue as  $\Delta \text{BIC}_{10}$ . Values  $>2$  represent a positive support for  $H_1$  (oscillator model) over  $H_0$  (no rhythm). Grey scale represents density estimate, scaled to a maximum of 1. Below the diagonal:  $\text{SWrc}$  values for genes co-expressed between tissues with non-overlapping 95% CIs. Note that  $\text{SWrc}$  values are expressed relative to the midpoint of the values obtained in the two tissues (i.e., 0-centering). See Table S1 for gene names.

the timing of gene expression, we fitted clock-gene expression in cortex and liver to a 24 h clock corresponding to the tissue's ZT in baseline (Figure 6B, dashed line) using a multivariate regression model with elastic net regularization.<sup>48</sup> We observed that during the SD and the subsequent 5 h of recovery (corresponding to ZT0–ZT11 in baseline), cortical local time no longer followed ZT and that the expression dynamics of clock genes was halted at a state corresponding to ZT0–ZT2 during baseline (Figure 6B, solid line). By contrast, in the liver, circadian time progressed undisturbed, resulting in a desynchronization between the two tissues with a maximum cortex-to-liver delay of 8 h reached 5 h after the end of the SD (Figure 6B, bottom).

As the cortical transcriptome, including most clock genes, is mostly sleep-wake driven, ZT (or circadian time defined by phase markers of the central circadian clock) has little significance in this tissue. That ZT estimated by the expression of clock genes was maintained at ZT0–ZT2 for 11 consecutive hours does therefore not indicate that the circadian clock stopped but simply results from the SD keeping waking levels high for 6 additional hours following the baseline dark period when animals were mostly awake spontaneously.

Because genes revealed a wide range of sleep-wake responses within each tissue (Figure 5), SD might also change intra-tissue synchronicity, i.e., the SD-induced change in each

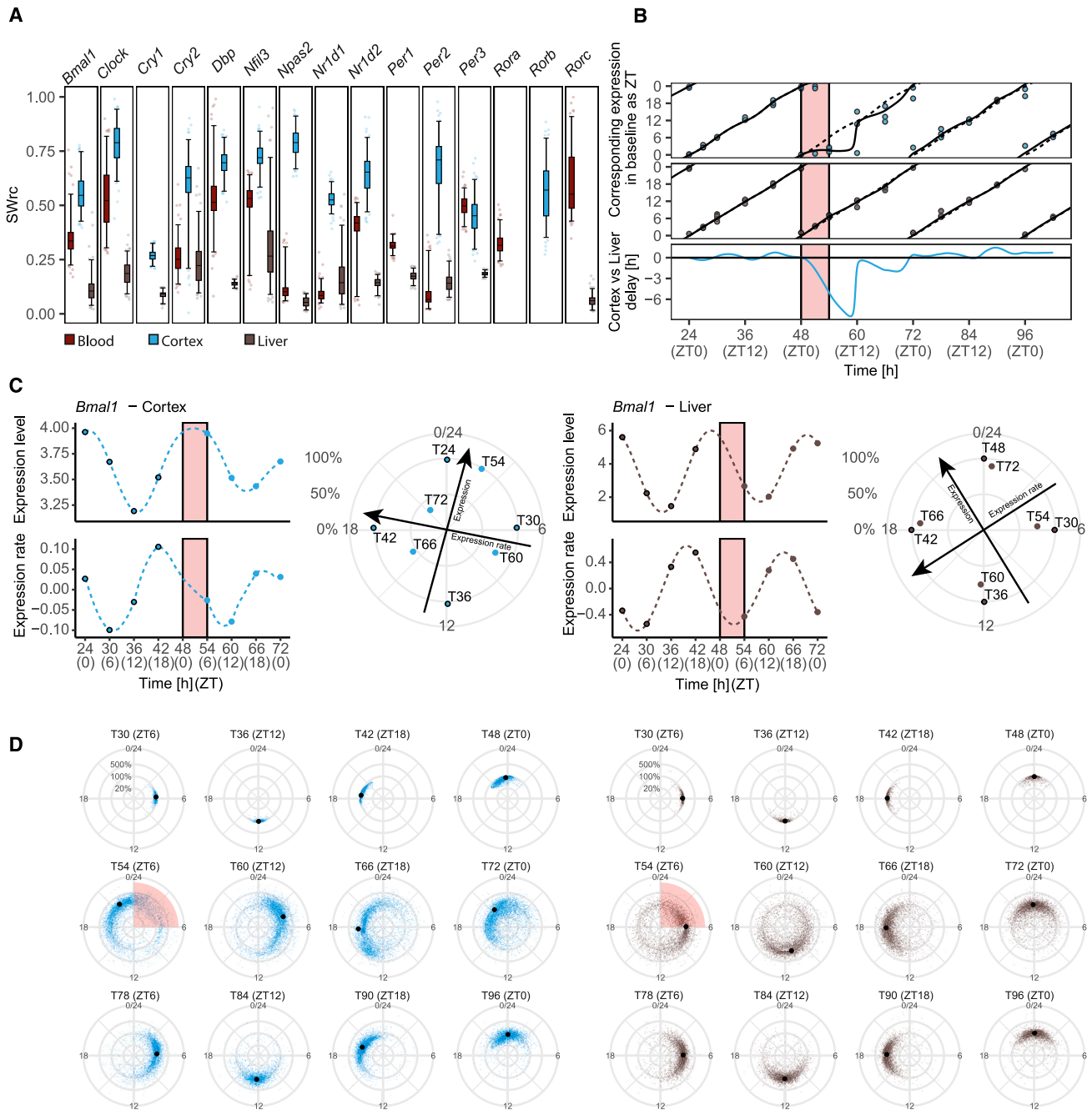


**Figure 6. SD changes timing of gene expression within and between tissues**

(A) Sleep-wake response contribution (*SWrc*;  $n = 200$  bootstraps per gene per tissue, and boxplots represent 95% bootstrap percentile confidence interval with 2.5%, 25%, 50%, 75%, and 97.5% percentiles) for clock-gene expression in mouse cortex (blue), liver (brown), and blood (red) in humans. In blood, *SWrc* was estimated from the top probes of the same clock genes (highest  $\Delta\text{BIC}_{10}$ ).

(B) Fitted and predicted local circadian time in cortex and liver based on clock-gene expression. The tissue's local time (expressed as zeitgeber time [ZT] in baseline; ZT0/ZT24, ZT3, ZT12, and ZT18) was fitted using baseline clock-gene expression with an elastic net model. Local time is then predicted for gene expression during SD (T51<sub>ZT3</sub> and T54<sub>ZT6</sub>) and subsequent recovery (REC, i.e., T60<sub>ZT12</sub>, T66<sub>ZT18</sub>, and T72<sub>ZT0</sub>). Projected fits based on our oscillator model as dashed (baseline) and solid (response to SD) lines. Lower graph depicts the cortex-liver tissue differences in predicted ZT.

(C) Estimated relative phase and amplitude of *Bmal1* from expression level and expression rate of the model. Baseline points T24/T48<sub>ZT0</sub>, T30<sub>ZT6</sub>, T36<sub>ZT12</sub>, and T42<sub>ZT18</sub> are fitted to a 24 h clock. Time on the horizontal axes is given both in time-of-experiment and ZT (in parentheses).

(D) Relative phase and amplitude of the expression of all rhythmic genes individually fitted to baseline (4 circular plots on upper row; from left-to-right: ZT6, ZT12, ZT18, and ZT24/ZT0) and their predicted ZT times for SD and recovery days 1 (middle) and 2 (lower rows) in cortex (left, blue dots;  $n = 91\%$  of 7,237 = 6,626) and liver (right, brown dots;  $n = 96\%$  of 5,770 = 5,539). Larger black dots represent the point of gravity of level and rate of expression of all genes.

transcript's phase relative to that of all other genes. To examine this, we performed a similar analysis as above, where the baseline timing of expression is estimated independently for each gene based on its expression level and expression rate predicted by our model. The baseline time points ZT0, ZT6, ZT12, and ZT18 were mapped onto ZT, and time points after the start of the SD were plotted according to baseline time considering expression level and expression rate (Figure 6C; see STAR Methods). In this representation, the distance from the center reflects a relative amplitude change (100% = baseline), and an angular change between corresponding ZT points before (baseline) and after SD ( $ZT_{SD}$  and  $ZT_{REC}$ ) can be viewed as a phase change.

SD caused extensive scattering of gene timing in both tissues, which lasted for more than 24 h (Figure 6D), indicating that the phase relationship among genes is largely altered by SD. Despite this increased scattering, the “point of gravity” of the timing of all transcripts in liver still closely followed baseline timing. By contrast, in the cortex, overall timing was impacted to a larger degree with points of gravity deviating from those observed in baseline by ca. 8 h at ZT6 and ZT12. It thus appears that the SD-induced changes in the cortical timing of expression level and expression change observed of clock genes (Figure 6B) apply to the entire rhythmic transcriptome in this tissue. On the second recovery day, scattering of timing remained larger than in baseline in both tissues, suggesting that the expression of many genes was still perturbed, although in the cortex, the location of the points of gravity suggests that overall, the timing had reverted to that of baseline (Figure 6D). The effects of SD on gene timing were not less pronounced for underdamped transcripts (Figure S5).

### Does recovery sleep accelerate transcriptome recovery?

We previously reported that the expression dynamics of a large number of genes affected by SD still deviated from baseline long after the sleep-wake distribution, and EEG activity had reverted to baseline, i.e., beyond the first 18 h after the SD ended<sup>14</sup> (see Figure 6D). Using our model prediction, we further investigated the “recovery” dynamics for the rhythmic transcripts affected by SD, i.e., those transcripts for which differential gene expression (SD/baseline fold-change) showed an effect size  $>1$  (Z score) at any time point during the 42 h after SD. We first determined how the fold-change in expression reached at the end of SD ( $ZT6_{SD}$ ) related to the time required for expression to again reach equilibrium, i.e., the time constant,  $\tau$  (Equation 4). Perhaps counterintuitively, we found that, in general, genes for which the expression was affected the most at the end of the SD had the shortest time constants (Figure 7A). More genes displayed such a strong-and-fast response in cortex than in liver where the initial responses tended to be smaller but longer lasting (Figure 7A).

The immediate SD effect and  $\tau$  alone were, however, insufficient to account for the large variability among genes and tissues in the time required for gene expression to return to its baseline rhythmicity (here referred to as recovery). One factor that could play a role is the extra sleep gained during recovery, which could be viewed as a second perturbation affecting the time to recover. To evaluate the effect of recovery sleep on transcriptome recov-

ery, we simulated gene expression in mice that do not (i.e., “0 h recovery sleep”) or partially compensate for sleep loss by incrementally (hour-by-hour) replacing the subsequent actual sleep-wake distribution by their ZT-matched baseline sleep (see Figure S6 for an example of baseline and recovery sleep-wake behavior in a mouse). Thus, with “0 h recovery,” the entire recovery sleep-wake pattern is replaced with that of baseline, with “1 h recovery” only the first hour of the actual recovery sleep-wake pattern is kept and the remainder replaced with that of baseline, and so forth, until again the actual 42 h recovery period was considered. We illustrate this analysis with the simulated expression of *Mfsd4a* and *Paqr8* with either 0, 6, 12, or 18 h of recovery sleep (Figures 7B and 7C, middle). We took these two genes because their cortical response to recovery sleep was opposite, while both tended to be sleep-wake driven ( $SWrc = 0.80$  and  $0.52$ ) and showed a comparable large effect size after SD ( $-7.0$  and  $+6.5$ , respectively at  $ZT6_{SD}$ ; Figures 7B and 7C, left). Moreover, *Mfsd4a* and *Paqr8* were under- and overdamped, respectively ( $\zeta = 0.76$  and  $3.17$ ). From the time point in the simulation when the actual recovery sleep was replaced with baseline sleep, the fold-change of underdamped genes (such as *Mfsd4a*) can be viewed as an underdamped oscillator relaxing back to equilibrium with its amplitude decaying exponentially with a time-constant  $\tau$  (red dashed lines in Figure 7B, middle; compare to *Gene A* in Figure 2B, left). For overdamped genes (such as *Paqr8*), the reduction in the fold-change follows a simple exponential decay (red dashed lines in Figure 7C, middle; see *Gene B* in Figure 2B, left). We then calculated the time required for the exponential decay part describing the recovery of gene expression to reach an effect size of  $<1$ , at which time point gene expression was considered to have recovered. We estimated that 50% of all genes affected by SD “recovered” within 12 and 13 h, and an additional 17% and 12% after 18 h of recovery, for cortex and liver, respectively (Figure 7D). This implies that at the time sleep and EEG phenotypes no longer differed from baseline, the expression of 32%–37% of genes still had not recovered. Using the baseline sleep-wake data instead of the actual sleep-wake recovery data accelerated the recovery of *Mfsd4a* expression by approximately 10 h, while it delayed *Paqr8*'s recovery by a similar duration (Figures 7B and 7C, middle). In other words, as more recovery sleep was included, time of recovery increased for *Mfsd4a* from 62 to 72.5 h when 10 h of recovery sleep was included and decreased for *Paqr8* expression (from 77.4 to 67.9 h) with 18 h of recovery sleep (Figures 7B and 7C, right). In general, overdamped ( $\log_{10} \zeta > 0$ ) genes, such as *Paqr8*, seemed to benefit from sleeping more (Figure 7E, green-black sequence, with green indicating that including more of recovery sleep accelerated gene recovery), whereas most genes with an oscillatory component (i.e., underdamped, like *Mfsd4a*) delayed their recovery time as more of the actual recovery sleep was being used for the simulation (Figure 7E, red-black sequence). We also observed more complex responses where recovery sleep initially decreases and subsequently increases recovery time (Figure 7E, green-red-black sequence). The opposite sequence could also be observed (Figure 7E, red-green-black sequence). Clustering the response of all genes revealed the presence of 6 types of responses (Figure 7E). In the cortex, recovery sleep delays gene recovery time for most of the clock genes. By contrast, several IEGs like

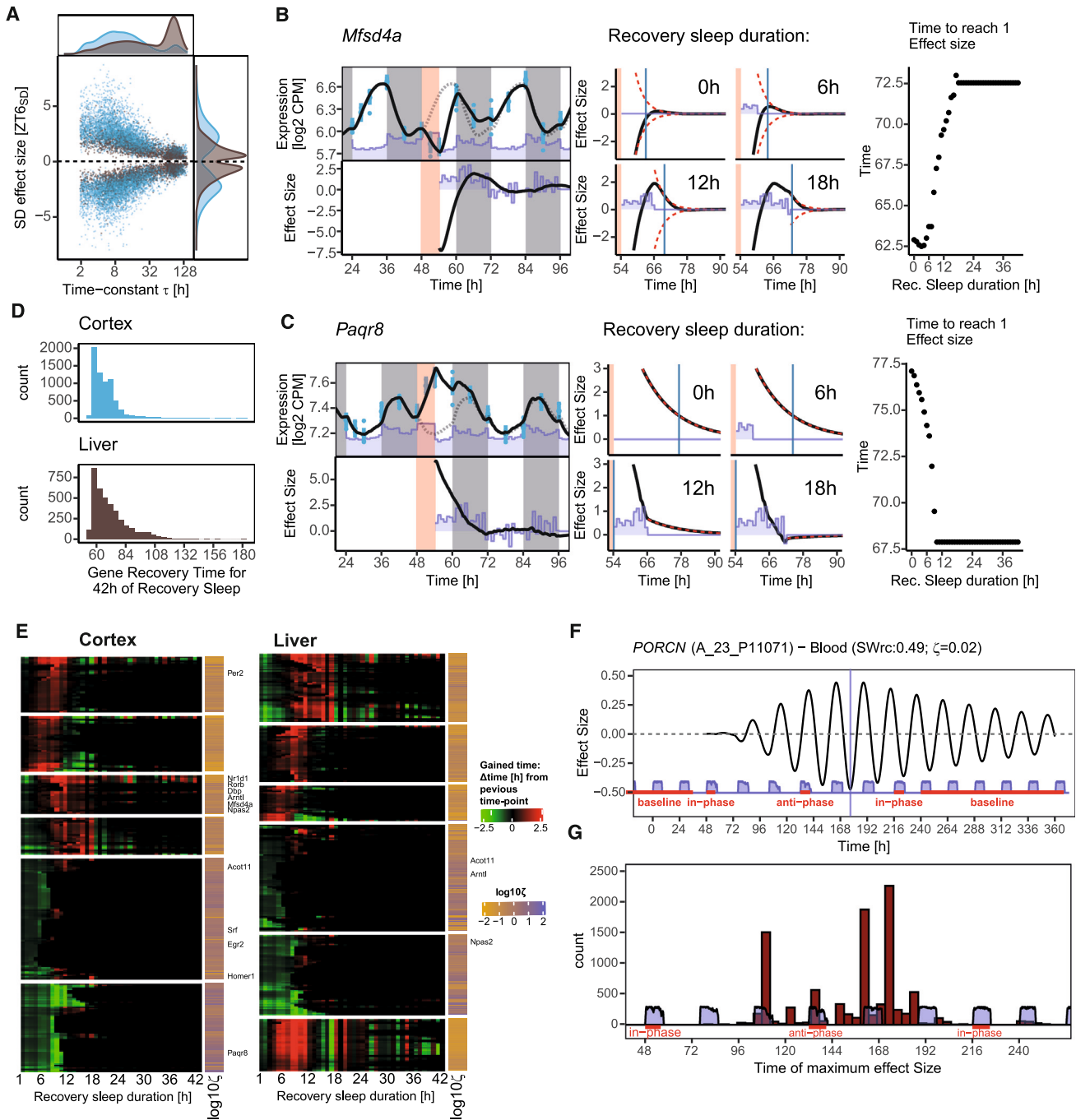


**Figure 7. Responses to recovery sleep**

(A) Effect size of differential gene expression at the end of sleep deprivation (SD; ZT6<sub>SD</sub> vs. ZT6 in baseline) vs. the model-derived recovery time-constant  $\tau$  in mouse liver (brown) and cortex (blue) for all rhythmic genes with a sleep-wake-driven contribution ( $SWrc > 0.25$ ;  $n = 3,872$  and  $6,891$ , respectively). Relative distributions for  $\tau$  and effect size plotted along their respective axes.

(B) Left: *Mfsd4a* expression (blue bars, 95% CI;  $n = 3-5$ /time point), its model fit (solid black line; dotted line replots baseline fit), and sleep-wake distribution (purple area; upper graph), with recovery vs. baseline effect size (black line) after SD and hourly values of sleep gain during recovery (purple area; lower graph). Center: effect size (black lines) when 0, 6, 12, or 18 h of the actual recovery sleep recording (as opposed to baseline sleep) was used for predicting gene expression after SD. Purple area indicates actual recovery sleep data included in each of the 4 simulations. Dashed red lines are the exponential parts of the oscillator solution when using only baseline sleep after SD (0 h recovery sleep; see Figure 2B, left). Blue vertical line marks the time point at which the exponential part reaches an effect size of  $+1.0$  or  $-1.0$ , which in subsequent analyses is considered the time at which gene expression has recovered. Right: time point of gene recovery when including 0–42 h of recovery sleep.

(C) As (B) but for *Paqr8*.

(legend continued on next page)

*Homer1*, *Srf*, and *Egr2* and others like *Acot11* take advantage of the extra sleep after SD to recover faster.

As transcriptome recovery can outlast sleep-wake recovery, we explored the transcriptome dynamics during the FD protocol during which subjects recover from transitioning from sleeping in-phase to anti-phase and back again by calculating the gene effect size of the predicted differential expression to corresponding baseline ZT time points. For each gene, we calculated the time point at which the effect size was highest. For example, for *PORCN*, a gene with a large effect size (top 2%) and extreme long time constant of recovery ( $\tau = 160$  h), the maximum effect size was reached at time 177 h (Figure 7F). The model predicted that for most genes, the largest effect sizes occurred around that time (144–192 h), i.e., during the 28 h day that followed the anti-phase condition (Figure 7G; days 7–8 of the protocol, Figure 2B). Such delayed response is reminiscent of the delayed gene-expression responses observed in mice after SD. The model also predicted that genes like *PORCN*, can still deviate from their baseline dynamics when sleep occurred again in-phase (Figure 7F).

## DISCUSSION

We have presented a mathematical framework that can describe and predict rhythmic gene expression in brain and body tissues peripheral to the SCN. The model integrates and quantifies the contributions of circadian and sleep-wake state related factors and their interaction acting on the daily changes in mRNA levels. The respective contributions of these factors were represented as two drives that each alter the acceleration of the ongoing changes in gene expression within the cells of the tissue. The model was able to capture the often complex and sometimes counterintuitive relationships between sleep-wake interventions, circadian time, and gene expression in cortex and liver in mice and in blood in humans. One strength of this driven harmonic oscillator is that it accommodates in a single mathematical model a variety of expression dynamics. This has the important advantage that parameter optimization will decide with which type of dynamics each gene responds to the exerted drives and which of the two drives is dominant. Moreover, although expression dynamics of individual genes might be fit better with simpler models, the use of a single model avoids having to determine the optimal model for each gene and tissue, which would render parameter comparison among genes or for the same genes among tissues impossible.

Although keeping the number of free parameters low, the model successfully captured changes in gene expression under a number of experimental conditions that altered sleep-wake timing relative to circadian timing. Applying the model to mouse

and human time course transcriptome data yielded several insights that are summarized below. Our work shows that the daily or circadian changes in *in vivo* gene expression can only be understood when both the contribution of sleep-wake history and circadian time are taken into account. We believe this framework to be useful not only to describe and predict the changes in gene expression under various experimental conditions affecting circadian time or sleep pressure but also that of other physiological variables and behaviors.

### More than one kind of sleep-wake-driven process

The effects of sleep loss on neurophysiology, performance, and behavior are often put into the context of the two-process model of sleep regulation<sup>49</sup> in which a sleep-wake-driven process, process S, increases and decreases during wakefulness and sleep, respectively, according to exponential saturating functions. As we showed here and elsewhere,<sup>14,15,43</sup> this type of dynamics captured well the changes in the cortical mRNA levels of IEGs characterized as overdamped in the model. Accordingly, expression of this class of genes responded to SD with a large, immediate increase, which then quickly decreased during sleep.

Our current analyses showed, however, that the response to the sleep-wake-driven factor of most predominantly sleep-wake-driven transcripts did not behave like process S. Instead, they followed a dynamic characterized with a small response at the end of SD, a slow recovery (17 h), and a larger variety of expression patterns, independent of their response to the circadian factor. Among these patterns, a marked inertia in the response to altered timing of sleep-wake state was observed, with differences in gene expression becoming evident only after some delay. This explains why these transcripts have gone unnoticed in experimental designs that aimed at finding the molecular correlates of process S and therefore only focused on the immediate effects of sleep loss. In modeling terms, these genes share the high *SWrc* with IEGs but differ in that damping ratio and natural frequency are low, resulting in large phase lags that together explain the inertia in the response to extended waking. The genes following these slower sleep-wake-driven dynamics might be implicated in the homeostatic regulation of time-spent-asleep, which differs from that of EEG delta power in that it has slower dynamics and becomes evident only after process S (and EEG delta power) has reverted to baseline.<sup>20</sup>

### Unexpected effects of recovery sleep on transcriptome recovery

Our analyses showed that deviations from the baseline sleep-wake state time course altered gene expression patterns. Perhaps counterintuitively, these deviations included rebound sleep subsequent to SD, which is generally considered to help

(D) Histogram of gene recovery time points for all rhythmic genes with a *SWrc* > 0.25 in cortex (upper, blue) and liver (lower, brown) using the actual (42 h) recovery sleep.

(E) Gain in gene recovery time for all genes in (D) in cortex (left) and liver (right). Analyses as in right-hand panels of (B) and (C), but here the differences from one time point to its preceding time point are plotted. As more sleep recovery recording was included in the simulation, genes either advanced (green) or delayed (red) their recovery time. Data were filtered to show only genes with a minimum of 1 h advance or delay.

(F) Effect size for differential *PORCN* expression (FD vs. baseline) for the expression simulated during the entire FD protocol and for 10 repetitions of baseline sleep-wake patterns under 24 h days after the second in-phase condition. Vertical blue line indicates the time when the maximum effect size was reached (time = 177 h).

(G) Time of maximum effect size modeled in the FD protocol for all rhythmic genes.

restore homeostatic balance. Rebound sleep especially affected the genes that responded with slower response dynamics and had an oscillatory component (i.e., underdamped) by delaying their recovery. The combination of the inertia to respond to enforced waking and their sensitivity to rebound sleep resulted in a flattening of rhythm amplitude that lasted well beyond the sleep-wake distribution, and EEG activity had reverted to baseline. The cortical expression pattern of most of the core clock genes followed this pattern. Please note that we have used the term gene expression recovery as shorthand for describing the time it took to again reach the baseline time course without knowing whether the transcripts indeed play a role in the recovery processes associated with sleep.

### Sleep loss leads to intra- and inter-tissue desynchronization of the transcriptome

Our analyses and model implementation showed that SD in the mouse caused a long-term change in the phase relationship among genes within and between tissues. Consistent with more genes being sleep-wake driven in cortex than in liver, SD impacted overall timing in cortex to a much larger extent, resulting in a large difference in circadian timing between the two tissues. The phase differences were observed at the level of the whole transcriptome as well as among clock genes. In cortex, but not in liver, all but one of the clock genes were affected by sleep-wake state with *Clock* and *Npas2* expression, the two transcription factors forming the positive arm of the circadian TTFL, responding, like IEGs, almost exclusively to the sleep-wake time course over the 4-day experiment. This tissue difference in the behavior of clock genes might not surprise given the fact that sleep-wake state is tightly coupled to metabolic activity in the cortex and less so in liver. The clock-gene circuitry in the cortex might thus be used to track and predict time-spent-awake instead of setting circadian time. Accordingly, clock genes in the cortex are of little significance as phase markers of the central circadian clock, as was already suggested by others for other tissues peripheral to the SCN.<sup>50</sup> To further investigate the relationship between the tissue's activity and clock-gene dynamics, one could, e.g., change (metabolic) activity of the liver specifically without affecting sleep-wake state. We predict that the expression dynamics of clock genes in the liver would become less circadian and more "cortex" like.

### STAR★METHODS

Detailed methods are provided in the online version of this paper and include the following:

- [KEY RESOURCES TABLE](#)
- [RESOURCE AVAILABILITY](#)
  - Lead contact
  - Materials availability
  - Data and code availability
- [EXPERIMENTAL MODEL AND STUDY PARTICIPANT DETAILS](#)
  - Mice
  - Participants in the Forced Desynchrony (FD)
  - Participants in the Constant Routine (CR)
- [METHOD DETAILS](#)
  - Mouse sleep deprivation
  - Mouse EEG/EMG recordings
  - Mouse tissue collection

- Mouse, RNA-sequencing
- Human, FD protocol
- Human, CR protocol
- Human, Polysomnography
- Human, RNA extraction, microarray hybridization
- [QUANTIFICATION AND STATISTICAL ANALYSIS](#)
  - Mouse, Gene quantification from RNA-seq
  - Human, Gene quantification from microarray
  - Derivation of the driven damped oscillator model
  - Solutions of the driven damped oscillator model
  - Process-S-like dynamics in the driven damped oscillator
  - Piecewise constant driving
  - Numerical solution
  - Model initial values and optimization procedure
  - Model Statistics
  - Model Comparisons
  - PCA analysis
  - Cortex and liver transcriptome timing

### SUPPLEMENTAL INFORMATION

Supplemental information can be found online at <https://doi.org/10.1016/j.cels.2024.06.005>.

### ACKNOWLEDGMENTS

We thank Nicolas Guex for his valuable comments on an earlier version of this manuscript and Aliénor Held for her input on the graphical abstract. M.J., S.J., and C.N.H. were supported through grants from the Swiss National Science Foundation (31003A\_173182 and 310030B\_192805 to P.F.). M.J. and P.F. were supported by the University of Lausanne and the Canton de Vaud, Switzerland. D.-J.D.'s research is supported by the UK Dementia Research Institute (award number UKDRI-7005) through UK DRI Ltd., principally funded by the UK Medical Research Council and the Alzheimer's Society as additional funding partners. The blood transcriptome data collection was funded through Air Force Office of Scientific Research grant FA9550-08-1-0080 and Biotechnology and Biological Sciences Research Council grant BB/F022883 to D.-J.D.

### AUTHOR CONTRIBUTIONS

M.J. and P.F. conceived and designed the project. P.F., C.N.H., and D.-J.D. designed the experiments on which the current analyses were based. C.N.H. and S.J. collected the new mouse data for this project, supervised by P.F. D.-J.D. made the human sleep and transcriptome data available for analyses. M.J. developed all scripts, performed all analyses, and generated all figures. A.C.S. contributed to formalizing the mathematical model. M.J. and P.F. wrote the manuscript. D.-J.D. and A.C.S. helped shape the story and contributed to all versions of the manuscript. All authors read and approved the final manuscript.

### DECLARATION OF INTERESTS

The authors declare no competing interests.

Received: August 17, 2023

Revised: April 15, 2024

Accepted: June 18, 2024

Published: July 9, 2024

### REFERENCES

1. Zhang, R., Lahens, N.F., Ballance, H.I., Hughes, M.E., and Hogenesch, J.B. (2014). A circadian gene expression atlas in mammals: implications for biology and medicine. *Proc. Natl. Acad. Sci. USA* *111*, 16219–16224. <https://doi.org/10.1073/pnas.1408886111>.
2. Mure, L.S., Le, H.D., Benegiamo, G., Chang, M.W., Rios, L., Jillani, N., Ngotho, M., Kariuki, T., Dkhissi-Benyahya, O., Cooper, H.M., and Panda, S. (2018). Diurnal transcriptome atlas of a primate across major

- neural and peripheral tissues. *Science* 359, eaao0318. <https://doi.org/10.1126/science.aao0318>.
3. Talamanca, L., Gobet, C., and Naef, F. (2023). Sex-dimorphic and age-dependent organization of 24-hour gene expression rhythms in humans. *Science* 379, 478–483. <https://doi.org/10.1126/science.add0846>.
  4. Takahashi, J.S. (2017). Transcriptional architecture of the mammalian circadian clock. *Nat. Rev. Genet.* 18, 164–179. <https://doi.org/10.1038/nrg.2016.150>.
  5. Dibner, C., Schibler, U., and Albrecht, U. (2010). The mammalian circadian timing system: organization and coordination of central and peripheral clocks. *Annu. Rev. Physiol.* 72, 517–549. <https://doi.org/10.1146/annurev-physiol-021909-135821>.
  6. Gerber, A., Saini, C., Curie, T., Emmenegger, Y., Rando, G., Gosselin, P., Gotic, I., Gos, P., Franken, P., and Schibler, U. (2015). The systemic control of circadian gene expression. *Diabetes Obes. Metab.* 17, 23–32. <https://doi.org/10.1111/dom.12512>.
  7. Koike, N., Yoo, S.H., Huang, H.C., Kumar, V., Lee, C., Kim, T.K., and Takahashi, J.S. (2012). Transcriptional architecture and chromatin landscape of the core circadian clock in mammals. *Science* 338, 349–354. <https://doi.org/10.1126/science.1226339>.
  8. Kinouchi, K., Mikami, Y., Kanai, T., and Itoh, H. (2021). Circadian rhythms in the tissue-specificity from metabolism to immunity: insights from omics studies. *Mol. Aspects Med.* 80, 100984. <https://doi.org/10.1016/j.mam.2021.100984>.
  9. Cirelli, C., Gutierrez, C.M., and Tononi, G. (2004). Extensive and divergent effects of sleep and wakefulness on brain gene expression. *Neuron* 41, 35–43. [https://doi.org/10.1016/s0896-6273\(03\)00814-6](https://doi.org/10.1016/s0896-6273(03)00814-6).
  10. Terao, A., Wisor, J.P., Peyron, C., Apte-Deshpande, A., Wurts, S.W., Edgar, D.M., and Kilduff, T.S. (2006). Gene expression in the rat brain during sleep deprivation and recovery sleep: an Affymetrix GeneChip study. *Neuroscience* 137, 593–605. <https://doi.org/10.1016/j.neuroscience.2005.08.059>.
  11. Hasan, S., Pradervand, S., Ahnaou, A., Drinkenburg, W., Tafti, M., and Franken, P. (2009). How to keep the brain awake? The complex molecular pharmacogenetics of wake promotion. *Neuropsychopharmacology* 34, 1625–1640. <https://doi.org/10.1038/npp.2009.3>.
  12. Diessler, S., Jan, M., Emmenegger, Y., Guex, N., Middleton, B., Skene, D.J., Ibberson, M., Burdet, F., Götz, L., Pagni, M., et al. (2018). A systems genetics resource and analysis of sleep regulation in the mouse. *PLoS Biol.* 16, e2005750. <https://doi.org/10.1371/journal.pbio.2005750>.
  13. Mongrain, V., Hernandez, S.A., Pradervand, S., Dorsaz, S., Curie, T., Hagiwara, G., Gip, P., Heller, H.C., and Franken, P. (2010). Separating the contribution of glucocorticoids and wakefulness to the molecular and electrophysiological correlates of sleep homeostasis. *Sleep* 33, 1147–1157. <https://doi.org/10.1093/sleep/33.9.1147>.
  14. Hor, C.N., Yeung, J., Jan, M., Emmenegger, Y., Hubbard, J., Xenarios, I., Naef, F., and Franken, P. (2019). Sleep-wake-driven and circadian contributions to daily rhythms in gene expression and chromatin accessibility in the murine cortex. *Proc. Natl. Acad. Sci. USA* 116, 25773–25783. <https://doi.org/10.1073/pnas.1910590116>.
  15. Maret, S., Dorsaz, S., Gurcel, L., Pradervand, S., Petit, B., Pfister, C., Hagenbuchle, O., O'Hara, B.F., Franken, P., and Tafti, M. (2007). Homer1a is a core brain molecular correlate of sleep loss. *Proc. Natl. Acad. Sci. USA* 104, 20090–20095. <https://doi.org/10.1073/pnas.0710131104>.
  16. Suzuki, A., Yanagisawa, M., and Greene, R.W. (2020). Loss of Arc attenuates the behavioral and molecular responses for sleep homeostasis in mice. *Proc. Natl. Acad. Sci. USA* 117, 10547–10553. <https://doi.org/10.1073/pnas.1906840117>.
  17. Tononi, G., and Cirelli, C. (2020). Sleep and synaptic down-selection. *Eur. J. Neurosci.* 51, 413–421. <https://doi.org/10.1111/ejn.14335>.
  18. Diering, G.H. (2023). Remembering and forgetting in sleep: selective synaptic plasticity during sleep driven by scaling factors Homer1a and Arc. *Neurobiol. Stress* 22, 100512. <https://doi.org/10.1016/j.ynstr.2022.100512>.
  19. Franken, P. (2013). A role for clock genes in sleep homeostasis. *Curr. Opin. Neurobiol.* 23, 864–872. <https://doi.org/10.1016/j.conb.2013.05.002>.
  20. Franken, P., and Dijk, D.J. (2024). Sleep and circadian rhythmicity as entangled processes serving homeostasis. *Nat. Rev. Neurosci.* 25, 43–59. <https://doi.org/10.1038/s41583-023-00764-z>.
  21. Noya, S.B., Colameo, D., Brüning, F., Spinnler, A., Mircsof, D., Opitz, L., Mann, M., Tyagarajan, S.K., Robles, M.S., and Brown, S.A. (2019). The forebrain synaptic transcriptome is organized by clocks but its proteome is driven by sleep. *Science* 366, eaav2642. <https://doi.org/10.1126/science.aav2642>.
  22. Archer, S.N., Laing, E.E., Möller-Levet, C.S., van der Veen, D.R., Bucca, G., Lazar, A.S., Santhi, N., Slak, A., Kabiljo, R., von Schantz, M., et al. (2014). Mistimed sleep disrupts circadian regulation of the human transcriptome. *Proc. Natl. Acad. Sci. USA* 111, E682–E691. <https://doi.org/10.1073/pnas.1316335111>.
  23. Maury, E., Hong, H.K., and Bass, J. (2014). Circadian disruption in the pathogenesis of metabolic syndrome. *Diabetes Metab.* 40, 338–346. <https://doi.org/10.1016/j.diabet.2013.12.005>.
  24. Roenneberg, T., and Mrosovsky, M. (2016). The circadian clock and human health. *Curr. Biol.* 26, R432–R443. <https://doi.org/10.1016/j.cub.2016.04.011>.
  25. Daan, S., Beersma, D.G., and Borbély, A.A. (1984). Timing of human sleep: recovery process gated by a circadian pacemaker. *Am. J. Physiol.* 246, R161–R183. <https://doi.org/10.1152/ajpregu.1984.246.2.R161>.
  26. Möller-Levet, C.S., Archer, S.N., Bucca, G., Laing, E.E., Slak, A., Kabiljo, R., Lo, J.C., Santhi, N., von Schantz, M., Smith, C.P., and Dijk, D.J. (2013). Effects of insufficient sleep on circadian rhythmicity and expression amplitude of the human blood transcriptome. *Proc. Natl. Acad. Sci. USA* 110, E1132–E1141. <https://doi.org/10.1073/pnas.1217154110>.
  27. Jan, M., Gobet, N., Diessler, S., Franken, P., and Xenarios, I. (2019). A multi-omics digital research object for the genetics of sleep regulation. *Sci. Data* 6, 258. <https://doi.org/10.1038/s41597-019-0171-x>.
  28. Archer, S.N., Möller-Levet, C.S., Laing, E.E., and Dijk, D.J. (2022). Mistimed sleep and waking activity in humans disrupts glucocorticoid signalling transcripts and SP1, but not plasma cortisol rhythms. *Front. Physiol.* 13, 946444. <https://doi.org/10.3389/fphys.2022.946444>.
  29. Masubuchi, S., Honma, S., Abe, H., Ishizaki, K., Namihira, M., Ikeda, M., and Honma, K. (2000). Clock genes outside the suprachiasmatic nucleus involved in manifestation of locomotor activity rhythm in rats. *Eur. J. Neurosci.* 12, 4206–4214.
  30. Abe, H., Honma, S., Namihira, M., Masubuchi, S., and Honma, K. (2001). Behavioural rhythm splitting in the CS mouse is related to clock gene expression outside the suprachiasmatic nucleus. *Eur. J. Neurosci.* 14, 1121–1128. <https://doi.org/10.1046/j.0953-816x.2001.01732.x>.
  31. Wakamatsu, H., Yoshinobu, Y., Aida, R., Moriya, T., Akiyama, M., and Shibata, S. (2001). Restricted-feeding-induced anticipatory activity rhythm is associated with a phase-shift of the expression of mPer1 and mPer2 mRNA in the cerebral cortex and hippocampus but not in the suprachiasmatic nucleus of mice. *Eur. J. Neurosci.* 13, 1190–1196. <https://doi.org/10.1046/j.0953-816x.2001.01483.x>.
  32. Curie, T., Maret, S., Emmenegger, Y., and Franken, P. (2015). In vivo imaging of the central and peripheral effects of sleep deprivation and suprachiasmatic nuclei lesion on PERIOD-2 protein in mice. *Sleep* 38, 1381–1394. <https://doi.org/10.5665/sleep.4974>.
  33. Deboer, T., Vansteensel, M.J., Détári, L., and Meijer, J.H. (2003). Sleep states after activity of suprachiasmatic nucleus neurons. *Nat. Neurosci.* 6, 1086–1090. <https://doi.org/10.1038/nn1122>.
  34. Challet, E., Turek, F.W., Laute, M., and Van Reeth, O. (2001). Sleep deprivation decreases phase-shift responses of circadian rhythms to light in the mouse: role of serotonergic and metabolic signals. *Brain Res.* 909, 81–91. [https://doi.org/10.1016/s0006-8993\(01\)02625-7](https://doi.org/10.1016/s0006-8993(01)02625-7).

35. Gekakis, N., Staknis, D., Nguyen, H.B., Davis, F.C., Wilsbacher, L.D., King, D.P., Takahashi, J.S., and Weitz, C.J. (1998). Role of the CLOCK protein in the mammalian circadian mechanism. *Science* 280, 1564–1569. <https://doi.org/10.1126/science.280.5369.1564>.
36. Zhang, Y., Li, Y., Niepel, M.W., Kawano, Y., Han, S., Liu, S., Marsili, A., Larsen, P.R., Lee, C.H., and Cohen, D.E. (2012). Targeted deletion of thioesterase superfamily member 1 promotes energy expenditure and protects against obesity and insulin resistance. *Proc. Natl. Acad. Sci. USA* 109, 5417–5422. <https://doi.org/10.1073/pnas.1116011109>.
37. Yin, L., and Lazar, M.A. (2005). The orphan nuclear receptor Rev-erbalpha recruits the N-CoR/histone deacetylase 3 corepressor to regulate the circadian Bmal1 gene. *Mol. Endocrinol.* 19, 1452–1459. <https://doi.org/10.1210/me.2005-0057>.
38. Alenghat, T., Meyers, K., Mullican, S.E., Leitner, K., Adeniji-Adele, A., Avila, J., Bućan, M., Ahima, R.S., Kaestner, K.H., and Lazar, M.A. (2008). Nuclear receptor corepressor and histone deacetylase 3 govern circadian metabolic physiology. *Nature* 456, 997–1000. <https://doi.org/10.1038/nature07541>.
39. Aninye, I.O., Matsumoto, S., Sidhaye, A.R., and Wondisford, F.E. (2014). Circadian regulation of Tshb gene expression by Rev-Erbalpha (NR1D1) and nuclear corepressor 1 (NCOR1). *J. Biol. Chem.* 289, 17070–17077. <https://doi.org/10.1074/jbc.M114.569723>.
40. Mistlberger, R.E., Bergmann, B.M., Waldenar, W., and Rechtschaffen, A. (1983). Recovery sleep following sleep deprivation in intact and suprachiasmatic nuclei-lesioned rats. *Sleep* 6, 217–233. <https://doi.org/10.1093/sleep/6.3.217>.
41. Herzog, E.D., Hermansteyne, T., Smyllie, N.J., and Hastings, M.H. (2017). Regulating the suprachiasmatic nucleus (SCN) circadian clockwork: interplay between cell-autonomous and circuit-level mechanisms. *Cold Spring Harb. Perspect. Biol.* 9, a027706. <https://doi.org/10.1101/cshperspect.a027706>.
42. Gerstner, J.R., Koberstein, J.N., Watson, A.J., Zaperro, N., Risso, D., Speed, T.P., Frank, M.G., and Peixoto, L. (2016). Removal of unwanted variation reveals novel patterns of gene expression linked to sleep homeostasis in murine cortex. *BMC Genomics* 17, 727. <https://doi.org/10.1186/s12864-016-3065-8>.
43. Curie, T., Mongrain, V., Dorsaz, S., Mang, G.M., Emmenegger, Y., and Franken, P. (2013). Homeostatic and circadian contribution to EEG and molecular state variables of sleep regulation. *Sleep* 36, 311–323. <https://doi.org/10.5665/sleep.2440>.
44. Hoekstra, M.M., Jan, M., Katsioudi, G., Emmenegger, Y., and Franken, P. (2021). The sleep-wake distribution contributes to the peripheral rhythms in PERIOD-2. *eLife* 10, e69773. <https://doi.org/10.7554/eLife.69773>.
45. Sneppen, K., Krishna, S., and Semsey, S. (2010). Simplified models of biological networks. *Annu. Rev. Biophys.* 39, 43–59. <https://doi.org/10.1146/annurev.biophys.093008.131241>.
46. Möller-Levet, C.S., Laing, E.E., Archer, S.N., and Dijk, D.J. (2022). Diurnal and circadian rhythmicity of the human blood transcriptome overlaps with organ- and tissue-specific expression of a non-human primate. *BMC Biol.* 20, 63. <https://doi.org/10.1186/s12915-022-01258-7>.
47. Reinke, H., and Asher, G. (2019). Crosstalk between metabolism and circadian clocks. *Nat. Rev. Mol. Cell Biol.* 20, 227–241. <https://doi.org/10.1038/s41580-018-0096-9>.
48. Braun, R., Kath, W.L., Iwanaszko, M., Kula-Eversole, E., Abbott, S.M., Reid, K.J., Zee, P.C., and Allada, R. (2018). Universal method for robust detection of circadian state from gene expression. *Proc. Natl. Acad. Sci. USA* 115, E9247–E9256. <https://doi.org/10.1073/pnas.1800314115>.
49. Borbély, A.A. (1982). A two process model of sleep regulation. *Hum. Neurobiol.* 1, 195–204.
50. Dijk, D.J., and Duffy, J.F. (2020). Novel approaches for assessing circadian rhythmicity in humans: a review. *J. Biol. Rhythms* 35, 421–438. <https://doi.org/10.1177/0748730420940483>.
51. Mang, G.M., and Franken, P. (2012). Sleep and EEG phenotyping in mice. *Curr. Protoc. Mouse Biol.* 2, 55–74. <https://doi.org/10.1002/9780470942390.mo110126>.
52. Hasan, S., Santhi, N., Lazar, A.S., Slak, A., Lo, J., von Schantz, M., Archer, S.N., Johnston, J.D., and Dijk, D.J. (2012). Assessment of circadian rhythms in humans: comparison of real-time fibroblast reporter imaging with plasma melatonin. *FASEB J.* 26, 2414–2423. <https://doi.org/10.1096/fj.11-201699>.
53. Lazar, A.S., Santhi, N., Hasan, S., Lo, J.C., Johnston, J.D., Von Schantz, M., Archer, S.N., and Dijk, D.J. (2013). Circadian period and the timing of melatonin onset in men and women: predictors of sleep during the weekend and in the laboratory. *J. Sleep Res.* 22, 155–159. <https://doi.org/10.1111/jsr.12001>.
54. Chen, S., Zhou, Y., Chen, Y., and Gu, J. (2018). fastp: an ultra-fast all-in-one FASTQ preprocessor. *Bioinformatics* 34, i884–i890. <https://doi.org/10.1093/bioinformatics/bty560>.
55. Dobin, A., Davis, C.A., Schlesinger, F., Drenkow, J., Zaleski, C., Jha, S., Batut, P., Chaisson, M., and Gingeras, T.R. (2013). STAR: ultrafast universal RNA-seq aligner. *Bioinformatics* 29, 15–21. <https://doi.org/10.1093/bioinformatics/bts635>.
56. Robinson, M.D., McCarthy, D.J., and Smyth, G.K. (2010). edgeR: a Bioconductor package for differential expression analysis of digital gene expression data. *Bioinformatics* 26, 139–140. <https://doi.org/10.1093/bioinformatics/btp616>.
57. Johnson, W.E., Li, C., and Rabinovic, A. (2007). Adjusting batch effects in microarray expression data using empirical Bayes methods. *Biostatistics* 8, 118–127. <https://doi.org/10.1093/biostatistics/kxj037>.
58. Ritchie, M.E., Phipson, B., Wu, D., Hu, Y., Law, C.W., Shi, W., and Smyth, G.K. (2015). limma powers differential expression analyses for RNA-sequencing and microarray studies. *Nucleic Acids Res.* 43, e47. <https://doi.org/10.1093/nar/gkv007>.
59. De Los Santos, H., Bennett, K.P., and Hurley, J.M. (2021). Mosaic: a joint modeling methodology for combined circadian and non-circadian analysis of multi-omics data. *Bioinformatics* 37, 767–774. <https://doi.org/10.1093/bioinformatics/btaa877>.
60. Spiess, A.N., and Neumeier, N. (2010). An evaluation of R2 as an inadequate measure for nonlinear models in pharmacological and biochemical research: a Monte Carlo approach. *BMC Pharmacol.* 10, 6. <https://doi.org/10.1186/1471-2210-10-6>.
61. Raftery, A.E. (1995). Bayesian model selection in social research. *Sociol. Methodol.* 25, 111–163. <https://doi.org/10.2307/271063>.
62. Lê, S., Josse, J., and Husson, F. (2008). FactoMineR: an R package for multivariate analysis. *J. Stat. Software* 25, 1–18. <https://doi.org/10.18637/jss.v025.i01>.
63. Josse, J., and Husson, F. (2016). missMDA: A package for handling missing values in multivariate data analysis. *J. Stat. Software* 70, 1–31. <https://doi.org/10.18637/jss.v070.i01>.

## STAR★METHODS

### KEY RESOURCES TABLE

REAGENT or RESOURCE	SOURCE	IDENTIFIER
<b>Deposited Data</b>		
C57BL/6J Liver RNA-seq	This paper	<a href="https://www.ncbi.nlm.nih.gov/geo/query/acc.cgi?acc=GSE262410">https://www.ncbi.nlm.nih.gov/geo/query/acc.cgi?acc=GSE262410</a>
C57BL/6J Cortical RNA-seq	Hor et al. <sup>14</sup>	<a href="https://www.ncbi.nlm.nih.gov/geo/query/acc.cgi?acc=GSE140345">https://www.ncbi.nlm.nih.gov/geo/query/acc.cgi?acc=GSE140345</a>
C57BL/6J Sleep recording	Diessler et al. <sup>12</sup>	<a href="https://doi.org/10.6084/m9.figshare.c.4421327">https://doi.org/10.6084/m9.figshare.c.4421327</a>
Human transcriptome, Forced Desynchrony (FD)	Archer et al. <sup>22</sup>	<a href="https://www.ncbi.nlm.nih.gov/geo/query/acc.cgi?acc=GSE48113">https://www.ncbi.nlm.nih.gov/geo/query/acc.cgi?acc=GSE48113</a>
Human transcriptome, Constant Routine (CR)	Möller-Levet et al. <sup>26</sup>	<a href="https://www.ncbi.nlm.nih.gov/geo/query/acc.cgi?acc=GSE39445">https://www.ncbi.nlm.nih.gov/geo/query/acc.cgi?acc=GSE39445</a>
Human Sleep recordings FD and CR	Möller-Levet et al. <sup>22</sup> ; Archer et al. <sup>26</sup>	<a href="https://doi.org/10.5281/zenodo.10974195">https://doi.org/10.5281/zenodo.10974195</a>
Processed data and results	This paper	<a href="https://doi.org/10.5281/zenodo.10974195">https://doi.org/10.5281/zenodo.10974195</a>
<b>Software and Algorithms</b>		
Oscillator model	This paper	<a href="https://doi.org/10.5281/zenodo.11198126">https://doi.org/10.5281/zenodo.11198126</a>
Rmarkdown Analysis	This paper	<a href="https://doi.org/10.5281/zenodo.11198112">https://doi.org/10.5281/zenodo.11198112</a>

### RESOURCE AVAILABILITY

#### Lead contact

Further information and requests for resources and reagents should be directed to and will be fulfilled by the lead contact, Paul Franken ([paul.fanken@unil.ch](mailto:paul.fanken@unil.ch)).

#### Materials availability

This study did not generate new unique reagents.

#### Data and code availability

- RNA-seq data and microarray data have been deposited at GEO and are publicly available as of the date of publication. Mouse sleep recording and de-identified human summary sleep recording have been deposited at Zenodo and are publicly available as of the date of publication. Accession numbers are listed in the [key resources table](#).
- Original code and processed data have been deposited at github and zenodo and are publicly available as of the date of publication. DOIs are listed in the [key resources table](#).
- Any additional information required to reanalyze the data reported in this paper is available from the [lead contact](#) upon request.

### EXPERIMENTAL MODEL AND STUDY PARTICIPANT DETAILS

#### Mice

62 male mice C57BL/6J were purchased from Charles River, France for RNA-sequencing of cortical and liver tissues. 12 male mice C57BL/6J were purchased from the University of Tennessee Health Science Center (Memphis, TN, United States of America) for EEG/EMG recording. Housing conditions for both sets of mice were identical. Mice were acclimated to our facility for 2-4 weeks prior experimental procedure and kept under 12h light-12h dark conditions. Both experimental procedures were performed at the age of 10-12 weeks and approved by the veterinary authorities of the state of Vaud (SCAV). No additional animal experiments were performed for this publication.

#### Participants in the Forced Desynchrony (FD)

Transcriptome data was obtained from 22 participants (mean  $\pm$  SD of age, 26.3  $\pm$  3.4 y; 11 males and 11 female). All participants were white, in good health, without reported sleep problems (Pittsburgh Sleep Quality Index  $\leq$  5), and homozygous for the PER3 VNTR polymorphism (rs57875989), with equal numbers of <sup>4/4</sup> and <sup>5/5</sup> carriers (11 each).

### Participants in the Constant Routine (CR)

Transcriptome data was obtained from 26 participants (mean  $\pm$  SD of age,  $27.5 \pm 4.3$  y; 14 males and 12 female). Participants were predominantly white (19/26), in good health, without reported sleep disorder (Pittsburgh Sleep Quality Index  $\leq 5$ ) and homozygous for PER3 VNTR polymorphism (*rs57875989*).

## METHOD DETAILS

### Mouse sleep deprivation

Sleep deprivation (SD) was performed by gentle handling<sup>51</sup> for 6h starting at light onset (zeitgeber time ZT0-6).

### Mouse EEG/EMG recordings

Surgery was performed 10 days prior baseline recording as described in Mang and Franken.<sup>51</sup> 10 days of EEG/EMG signals were annotated on 4s consecutive epochs based on EEG/EMG pattern. Manual annotation was performed on day 3 of the recording which includes the SD, other days were annotated using a semiautomated scoring system.<sup>12,27</sup>

### Mouse tissue collection

Mice were anesthetized with isoflurane prior to decapitation. Cortex and liver were rapidly dissected, and flash frozen in liquid nitrogen. Time schedule of tissue sampling was described.<sup>14</sup>

### Mouse, RNA-sequencing

Frozen cortex samples were processed as described in Hor et al.<sup>14</sup> Liver samples were stored at  $-140^{\circ}\text{C}$  and prepared as follows: total RNA was extracted using miRNeasy kit (Qiagen; Hilden, Germany). Libraries were prepared using 10 ng/ $\mu\text{l}$  with Truseq Stranded RNA. Sequencing was performed on the Illumina HiSeq 4000 SR sequencer with more than 24 million reads per sample.

### Human, FD protocol

Participants underwent a first 8h baseline sleep schedule at habitual bedtime followed by a 28h sleep-wake cycle. Dark-dim light ( $<5$  lux) cycle and meals also followed a 28h cycle. Plasma melatonin levels were measured as described in Hasan et al.<sup>52</sup> to assess circadian period *in-vivo* and to schedule sleep to be in-phase with melatonin levels.<sup>53</sup> The protocol received a favorable opinion from the University of Surrey Ethics Committee and was conducted in accordance with the principles of the Declaration of Helsinki. They all provided written informed consent.

### Human, CR protocol

Participants had to stay awake for 39–41h on their bed, in their individual room in a semi-recumbent position under a low light intensity  $<10$  lux. Hourly nutritional drinks were provided instead of meals. Blood samples were collected hourly to assess melatonin levels and every 3h for total RNA extraction. The protocol received a favorable opinion from the University of Surrey Ethics Committee and was approved by the Institutional Review Board of the Air Force Research Laboratory. The study was conducted in accordance with the principles of the Declaration of Helsinki. All participants provided written informed consent after receiving a detailed explanation of the aims and procedures of the study and before any procedures described in the study.

### Human, Polysomnography

The EEG, EMG, and EOG (electro-oculogram) were recorded on Siesta 802 devices at a 256Hz sampling rate. After signal filtering, sleep stages were assessed according to the Rechtschaffen and Kales criteria. Participants' sleep was aligned using their melatonin phase and mean sleep amount was calculated using NREM sleep (stages 1–4) + REM sleep and considered baseline sleep onset as 'ZT0' in figures.

### Human, RNA extraction, microarray hybridization

Whole peripheral blood was collected using PAXgene Blood RNA tubes. cRNA was hybridized on a 4x44K custom oligonucleotide microarray with additional probes for 20 clock/sleep-related genes.

## QUANTIFICATION AND STATISTICAL ANALYSIS

### Mouse, Gene quantification from RNA-seq

Gene quantification was performed as follows for both cortex and liver samples: Illumina reads were filtered using fastp<sup>54</sup> to keep high quality reads and remove adapter sequences. Reads were aligned on the mouse reference genome mm10 (GRCm38) using STAR v2.7.0e<sup>55</sup> with default parameters. Read counts was done by STAR using "--quantMode GeneCounts", taking only reverse strand mapped reads. Genes with low counts (mean counts overall samples  $< 10$ ) were filtered and normalization was performed with edgeR.<sup>56</sup> Gene expression from the liver was put on Gene Expression Omnibus (GEO). Batch effects were removed using Combat<sup>57</sup> prior fitting using our model.

### Human, Gene quantification from microarray

Quality control and processing were performed with R package limma.<sup>58</sup> Probes intensities were corrected for background and Quantile normalized. Outliers detected with arrayQualityMetrics function and PCA were removed (3/714 samples). For both protocols, blood samples time-point were aligned using participant melatonin phase (i.e., defined as ‘time point’ in FD dataset metadata, and ‘circadian phase’ in CR dataset metadata). Probes were corrected for repeated measure on the same participant using a mixed-model with a random participant intercept and fixed effects of sleep condition (in-phase, anti-phased, 6h sleep + CR, 10h sleep + CR) and time points.

### Derivation of the driven damped oscillator model

Our goal was to develop a simple model which had the ability to exhibit both exponential and oscillatory behavior. The driven damped harmonic oscillator model is one such model. Here we add additional details to further explain how the driven damped harmonic oscillator equation can result from a simple model of the interaction of a gene with its environment and external driving factors. In the manuscript we state

$$\begin{aligned}\frac{dX}{dt} &= \alpha Y - \gamma X, \\ \frac{dY}{dt} &= -\beta X + F(t),\end{aligned}\tag{Equation 8}$$

where  $X(t)$  is the level of mRNA of a gene,  $Y(t)$  is a combination of intra-tissue factors which we term ‘tissue environment’, and  $F(t)$  captures external driving factors including sleep and wake and circadian rhythmicity. The constants  $\alpha, \beta, \gamma$  describe the effect of the environment on the gene, the effect of the gene on the environment and the gene degradation rate respectively.

We let  $X(t) = X_b + x(t)$ ,  $Y(t) = Y_b + y(t)$ ,  $F(t) = F_b + f(t)$ , where  $x(t), y(t), f(t)$  model the deviation from a stationary baseline. Substituting  $X(t), Y(t), F(t)$  into Equation 8 gives

$$\begin{aligned}\frac{dx}{dt} &= \alpha y - \gamma x + (\alpha Y_b - \gamma X_b), \\ \frac{dy}{dt} &= -\beta x + f(t) + (-\beta X_b + F_b).\end{aligned}\tag{Equation 9}$$

Since the stationary baseline values satisfy Equation 8 with  $dX/dt = dY/dt = 0$ , the terms in the brackets on the right-hand side of Equation 9 are zero, leaving

$$\frac{dx}{dt} = \alpha y - \gamma x,\tag{Equation 10}$$

$$\frac{dy}{dt} = -\beta x + f(t).\tag{Equation 11}$$

We note that while we would expect  $X(t) > 0$ ,  $x(t)$  may be positive or negative.

Now, differentiating Equation 10 with respect to time gives

$$\frac{d^2x}{dt^2} = \alpha \frac{dy}{dt} - \gamma \frac{dx}{dt}$$

Substituting for  $dy/dt$  from Equation 11 and re-arranging gives

$$\frac{d^2x}{dt^2} + \gamma \frac{dx}{dt} + \alpha\beta x = \alpha f(t)$$

i.e., the equation of a damped oscillator with natural frequency  $\omega_0 = \sqrt{\alpha\beta}$  driven by  $\alpha f(t)$

### Solutions of the driven damped oscillator model

Consider the driven damped harmonic oscillator

$$\frac{d^2x}{dt^2} + \gamma \frac{dx}{dt} + \omega_0^2 x = C + F_1 \cos \omega t + F_2 \sin \omega t,\tag{Equation 12}$$

with initial conditions

$$x(0) = \alpha, \left. \frac{dx}{dt} \right|_{t=0} = \beta,$$

where we note that the right-hand side of Equation 12 could alternatively be written as

$$C + A \sin(\omega t + \varphi)$$

where  $F_1 \equiv A \sin \varphi$ ,  $F_2 \equiv A \cos \varphi$ . Solutions to Equation 12 may be found using standard methods of calculus and consist of a linear combination of the 'complementary function'  $x_{CF}(t)$ , which is the solution to the homogeneous equation, namely

$$\frac{d^2x}{dt^2} + \gamma \frac{dx}{dt} + \omega_0^2 x = 0 \quad (\text{Equation 13})$$

and the 'particular integral' which is one solution to the inhomogeneous Equation 12. Here we separate the particular integral into two parts,  $x_h$  and  $x_c(t)$  where  $x_h$  is the consequence of a constant driving term  $C$  and  $x_c(t)$  is the consequence of the oscillatory driving term  $F_1 \cos \omega t + F_2 \sin \omega t$ . Hence the solution to Equation 12 takes the form

$$x(t) = x_{CF}(t) + x_h + x_c(t). \quad (\text{Equation 14})$$

The particular solution for the constant driving term is given by

$$x_h = \frac{C}{\omega_0^2}, \quad (\text{Equation 15})$$

and that for the two oscillatory terms as

$$x_c = D \cos \omega t + E \sin \omega t \equiv F \sin(\omega t + \tilde{\varphi}), \quad (\text{Equation 16})$$

where

$$D = \frac{(\omega_0^2 - \omega^2)F_2 - \gamma\omega F_1}{\gamma^2\omega^2 + (\omega_0^2 - \omega^2)^2}$$

$$E = \frac{\gamma\omega F_2 + (\omega_0^2 - \omega^2)F_1}{\gamma^2\omega^2 + (\omega_0^2 - \omega^2)^2} \quad (\text{Equation 17})$$

and  $F = \sqrt{D^2 + E^2}$ ,  $\tan \tilde{\varphi} = D/E$ .

The solution to the homogeneous equation,  $x_{CF}$ , separates into three types depending on the sign of  $\gamma^2 - 4\omega_0^2$ . Specifically, if  $\gamma^2 - 4\omega_0^2 > 0$ , solutions are 'overdamped' and

$$x_{CF} = A_o e^{a_1 t} + B_o e^{a_2 t}, \quad (\text{Equation 18})$$

where

$$a_{1,2} = \frac{-\gamma \pm \sqrt{\gamma^2 - 4\omega_0^2}}{2}$$

are real and negative.

If  $\gamma^2 = 4\omega_0^2$ , solutions are 'critically damped',

$$x_{CF} = (A_c t + B_c) e^{-\gamma t/2}. \quad (\text{Equation 19})$$

Finally, if  $\gamma^2 - 4\omega_0^2 < 0$ , solutions are 'underdamped',

$$x_{CF} = (A_u \cos \omega_1 t + B_u \sin \omega_1 t) e^{-\gamma t/2} \quad (\text{Equation 20})$$

where  $\omega_1^2 = \omega_0^2 - \gamma^2/4$ . We note that it is a matter of convention that the solutions for the overdamped and underdamped cases are written as exponential and trigonometric functions, respectively. Specifically, solutions for the underdamped case may be written in the form of Equation 19 but with  $a_{1,2}$  complex instead of real. Similarly, the overdamped case may be written in the form of Equation 19 but the frequency  $\omega_1$  will be imaginary instead of real. The fact that the two forms are equivalent is relevant for our separation of circadian and sleep-wake effects described below, as it means that a single formulation covers both cases.

Values for the constants  $A_o, B_o$  or  $A_c, B_c$  or  $A_u, B_u$  may be found using the initial conditions. For example:

$$A_u = \alpha - \frac{C}{\omega_0^2} - D,$$

$$B_u = \frac{\beta + \frac{\gamma}{2} \left( \alpha - \frac{C}{\omega_0^2} - D \right) - \omega E}{\omega_1}$$

Hence, the solution is completely determined by the seven constants in Equation 12 namely the damping parameters  $\gamma$ , the natural frequency  $\omega_0$ , the size of the constant driving term  $C$ , the two parameters specifying the sinusoidal driving term, either the amplitude and phase ( $A$  and  $\varphi$ ) or equivalently  $F_1$  and  $F_2$  and the two values specifying the initial conditions  $\alpha$  and  $\beta$ . The solution consists of three parts, where  $x_h$  is a constant,  $x_c(t)$  is oscillatory with a fixed amplitude and phase. In the underdamped case  $x_{CF}(t)$ , is a damped oscillatory term (see Equation 20) so

$$x(t) = x_{CF}(t) + x_h + x_c(t) = (A_u \cos \omega_1 t + B_u \sin \omega_1 t) e^{-\gamma t/2} + \frac{C}{\omega_0^2} + D \cos \omega t + E \sin \omega t \quad (\text{Equation 21})$$

In the overdamped case  $x_{CF}(t)$  is non-oscillatory (see Equation 19), and instead the general solution takes the form

$$x(t) = A_o e^{a_1 t} + B_o e^{a_2 t} + \frac{C}{\omega_0^2} + D \cos \omega t + E \sin \omega t. \quad (\text{Equation 22})$$

Finally, in the critically damped case the general solution takes the form

$$x(t) = (A_c t + B_c) e^{-\gamma t/2} + \frac{C}{\omega_0^2} + D \cos \omega t + E \sin \omega t. \quad (\text{Equation 23})$$

### Process-S-like dynamics in the driven damped oscillator

Process-S-like sleep-wake driven processes are usually described as exponential functions of the form

$$S(t) = \tilde{C} - (\tilde{C} - S_0) e^{-kt}$$

where  $S(t)$  is homeostatic sleep pressure,  $\tilde{C}$  is the asymptote i.e.  $S(t) \rightarrow \tilde{C}$  as  $t \rightarrow \infty$ ,  $k$  is the decay rate and  $S(t) = S_0$  at  $t = 0$ . In the absence of a sinusoidal driving term, the solution for the critically damped driven oscillator, given in Equation 23, reduces to  $S(t)$  for the initial conditions  $x(0) = S_0$  and  $x'(0) = k(\tilde{C} - S_0)$ .

### Piecewise constant driving

Sleep is assumed to result in a piecewise constant driving term, such that for  $t \in (t_{n-1}, t_n)$ , where  $n$  is the interval number  $n = 1, 2, \dots$  it takes the value  $C_n$  where the magnitude of the  $C_n$  is directly proportional to the fraction of time asleep. Taking the initial conditions for the  $n^{\text{th}}$  interval as

$$x(t_{n-1}) = \alpha_{n-1}, \quad \left. \frac{dx}{dt} \right|_{t=t_{n-1}} = \beta_{n-1}$$

and using Equation 12, then for the underdamped case the solution for  $x(t)$  in the  $n^{\text{th}}$  interval,  $x_n(t)$ , has the general form

$$x_n(t) = (A_n \cos \omega_1 t + B_n \sin \omega_1 t) e^{-\gamma t/2} + \frac{C_n}{\omega_0^2} + D \cos \omega t + E \sin \omega t, \quad (\text{Equation 24})$$

where  $D$  and  $E$  are

$$D = \frac{(\omega_0^2 - \omega^2) F_2 - \gamma \omega F_1}{\gamma^2 \omega^2 + (\omega_0^2 - \omega^2)^2} \quad \text{and} \quad E = \frac{\gamma \omega F_2 + (\omega_0^2 - \omega^2) F_1}{\gamma^2 \omega^2 + (\omega_0^2 - \omega^2)^2}, \quad (\text{Equation 25})$$

as in Equation 17  $A_n$  and  $B_n$  satisfy the linear simultaneous equations

$$\begin{aligned} \alpha_{n-1} &= (A_n \cos \omega_1 t_{n-1} + B_n \sin \omega_1 t_{n-1}) e^{-\gamma t_{n-1}/2} + \frac{C_n}{\omega_0^2} + D \cos \omega t_{n-1} + E \sin \omega t_{n-1}, \\ \beta_{n-1} &= -\frac{\gamma}{2} (A_n \cos \omega_1 t_{n-1} + B_n \sin \omega_1 t_{n-1}) e^{-\gamma t_{n-1}/2} + (-\omega_1 A_n \sin \omega_1 t_{n-1} + \omega_1 B_n \cos \omega_1 t_{n-1}) e^{-\gamma t_{n-1}/2} - \omega D \sin \omega t_{n-1} + \omega E \cos \omega t_{n-1}. \end{aligned} \quad (\text{Equation 26})$$

Solving Equation 26 gives

$$\begin{aligned} A_n &= \frac{e^{\gamma t_{n-1}/2}}{\omega_1} \left\{ \left( -\frac{\gamma}{2} \sin \omega_1 t_{n-1} + \omega_1 \cos \omega_1 t_{n-1} \right) \left( \alpha_{n-1} - \frac{C_n}{\omega_0^2} \right) - \sin \omega_1 t_{n-1} \beta_{n-1} + \left( \frac{\gamma}{2} \sin \omega_1 t_{n-1} - \omega_1 \cos \omega_1 t_{n-1} \right) \right. \\ &\quad \left. \times (D \cos \omega t_{n-1} + E \sin \omega t_{n-1}) - \omega \sin \omega_1 t_{n-1} (D \sin \omega t_{n-1} - E \cos \omega t_{n-1}) \right\} \end{aligned}$$

$$B_n = \frac{e^{\gamma t_{n-1}/2}}{\omega_1} \left\{ \left( \frac{\gamma}{2} \cos \omega_1 t_{n-1} + \omega_1 \sin \omega_1 t_{n-1} \right) \left( \alpha_{n-1} - \frac{C_n}{\omega_0^2} \right) + \cos \omega_1 t_{n-1} \beta_{n-1} - \left( \frac{\gamma}{2} \cos \omega_1 t_{n-1} + \omega_1 \sin \omega_1 t_{n-1} \right) \right. \\ \left. \times (D \cos \omega t_{n-1} + E \sin \omega t_{n-1}) + \omega \cos \omega_1 t_{n-1} (D \cos \omega t_{n-1} - E \sin \omega t_{n-1}) \right\} \quad (\text{Equation 27})$$

Hence, given  $\omega_0$ ,  $\gamma$ , a constant  $C$  which relates fraction of time asleep to the piecewise constant drive i.e.,  $C_n = C \times$  fraction of time asleep, the amplitude  $A$ , phase  $\varphi$  and angular frequency  $\omega$  (here,  $2\pi/24$  radians / hour) of the oscillatory driving term the solution is calculated as follows:

- From  $\omega_0$  and  $\gamma$  calculate  $\omega_1 = \sqrt{(\omega_0^2 - \gamma^2)}$
- From  $A$  and  $\varphi$  calculate the values of  $F_1$  and  $F_2$  since  $F_1 = A \sin \varphi$ ,  $F_2 = A \cos \varphi$
- Calculate  $D$  and  $E$  from Equation 25.
- Work iteratively through each time interval, starting at  $t_0$ . For each interval the solution  $x_n(t)$  is derived by evaluating  $A_n, B_n$ , using Equation 27. Once  $x_n(t)$  is found, the starting conditions  $\alpha_n$  and  $\beta_n$  for the next interval may be found by evaluating  $x_n(t_n)$  and  $x'_n(t_n)$  where  $x'_n(t_n)$  is the derivative of  $x_n(t_n)$  with respect to time.

To start this iterative process, values for  $\alpha_0$  and  $\beta_0$  are required. To ensure that the results were insensitive to the choice of  $\alpha_0$  and  $\beta_0$ , the sleep and circadian drives were prepended by 20 replicates of the baseline day.

The five required constants  $\omega_0$ ,  $\gamma$ ,  $C$ ,  $A$  and  $\varphi$  could be found by fitting the analytical solution to the gene expression data. In practice, these constants were evaluated instead by numerically integrating the oscillator equations using a fourth order Runge-Kutta method with a fixed step size. For a given set of constants, the numerical solution and the analytical solution matched to a high degree of accuracy (typical error less than  $10^{-7}$ , close to the precision of the variables), suggesting that any numerical errors are negligible. We note that the fitting was done with a piecewise constant sleep-wake drive, which in the  $n^{\text{th}}$  interval is given by  $\beta_W W_n(t) + \beta_S S_n(t)$  rather than using a sleep drive, as described in the analytical solution above. However, it is straightforward to transform between the two alternatives since in each 0.1 h interval the mouse is either asleep or awake, so  $W_n(t) + S_n(t) = 1$ . Hence the sleep-wake drive may alternatively be formulated as a constant plus sleep drive, i.e.,  $\beta_W + (\beta_W - \beta_S) S_n(t)$ .

The numerical solution yields a single fitted time series for each gene. The analytical solution then enables that single time trace to be separated into components driven by the different driving terms equivalent to the  $x_{CF}(t)$ ,  $x_h$  and  $x_c(t)$  in Equation 21. Specifically, the term  $x_c(t)$  is the response to the oscillatory drive. The term  $x_h$  is a response to the (piecewise) constant drive. The  $x_{CF}(t)$  is normally termed as the 'transient' since  $x_{CF}(t) \rightarrow 0$  as  $t \rightarrow \infty$ . Here, we find that  $x_{CF}(t)$  responds to the short timescale changes in fraction of time asleep so is not negligible. Consequently, in decomposing the fitted timeseries into circadian and sleep-wake driven contributions, we consider that circadian contributions are given by  $x_c(t)$  and sleep-wake state contributions are given by  $x_h + x_{CF}(t)$ .

The method used to calculate  $\omega_1, D, E, \alpha_n, \beta_n, A_n$  and  $B_n$  was described above for the underdamped case and coded in MATLAB and R. The same piece of code also worked for the overdamped case since, as discussed above, it is a matter of convention rather than a fundamental difference in the mathematical formula that distinguishes the two cases.

### Numerical solution

To find optimal parameters for the dynamics of each gene expression we (repeatedly) numerically integrated the driven harmonic oscillator. We first transformed the second order ordinary differential equation (ODE) into two first order ODEs,

$$x'_1 = x_2$$

$$x'_2 = F - \gamma x_2 - \omega_0^2 x_1$$

where  $x_1$  and  $x_2$  represents normalized mRNA counts and the prime (') indicates differentiation with respect to time. We then implemented a 4<sup>th</sup> order Runge-Kutta (RK4) numerical method to approximate the solution using a fixed time step of 0.1 hour. With a fixed step size of 0.1 hour, RK4 requires values every 0.05 hours.

### Model initial values and optimization procedure

The equilibrium position of the model was set as follows. For each gene or probe, we fitted a cosine to the baseline gene expression (Time 24–48 in mice, FD: in-phase in human) and used the intercept of the model as the default equilibrium position. Initial values of position  $x_1(0)$  and speed  $x_2(0)$  were set at the equilibrium position of the model and at 0, respectively. The baseline sleep-wake cycle (mean baseline sleep in mice, habitual bedtime in human) was repeated for 20 days prior recordings to let the model reach steady state. In humans, an extra free parameter was set for the oscillator equilibrium position in the CR experiment to consider mean difference between FD and CR. This effect could not be corrected in microarray processing directly as no RNA sampling point overlap between experiments, but can be corrected with our model as habitual bedtime sleep are comparable between FD and CR.

Optimization was performed using the box-constrained PORT routines method (nlminb) implemented in the optimx/R package. Optimization was done by minimizing the Residual Sum of Square (RSS) between the fit of the model and the expression value of the gene/probe analyzed. We fixed a lower and upper bound for each parameter:  $\beta_W$  and  $\beta_S$  bounds were set from 0–10 and

-10-0 (also tested for opposite effect).  $\omega_0$  bound was set from  $2\pi/72$  to  $2\pi/12$  (to avoid fitting oscillation frequencies too high with respect to gene expression sampling rate),  $\gamma$  bound was set from 0.01 to 100,  $A$  and  $\varphi$  bounds were set from 0 to 10 and 0 to  $2\pi$ . A penalization procedure of the  $RSS$  during the optimization was performed to avoid unstable fit in baseline and thus to ensure a steady state of the oscillator model. The maximal and minimal value ( $y_{tmax}$  and  $y_{tmin}$ ) of the oscillator (i.e., the fitted expression) in the 24h of baseline prior to the SD, FD, and CR experiments were compared with the level of the oscillator at the same 2 time-points during replicated baselines, according to  $RSS = RSS + \lambda (y_{tmax} - y_{tmax-24})^2 + \lambda (y_{tmin} - y_{tmin-24})^2$  with  $\lambda = 1000$ . The procedure was performed for up to 5 replicate baseline days prior to the baseline of the SD, FD, and CR experiments. This penalization was only applied for parameter optimization and not for computing model statistics.

### Model Statistics

Goodness of fit was estimated using Kendall's  $\tau$  ranked correlation between model fit and expression values. Kendall's  $\tau$  was used as  $R^2$  is inadequate for nonlinear regression of time series.<sup>59,60</sup> Bayesian Information Criterion ( $BIC$ ) of the model was calculated from the Negative log likelihood ( $NLL$ ), assuming that model residuals were independent and followed a Gaussian distribution.

$$RSS = \sum_{i=1}^n (y_i - \hat{y}_i)^2,$$

$$NLL = \left(\frac{n}{2}\right) * \left(\log(2\pi) + \log\left(\frac{RSS}{n}\right) + 1\right),$$

$$BIC = -2(-NLL) + k \log(n).$$

Where  $n$  is the number of samples,  $y_i$  the gene expression value at time-point  $i$ , and  $k$  the number of free parameters of the model + 1 (the biased estimator of the error variance  $\sigma_\epsilon^2$ ). For our model ( $H_1$ ):  $k = 7$  for mouse dataset and  $k = 8$  for human dataset. For the flat model ( $H_0$ ):  $k=2$  for mouse dataset and  $k=3$  for human dataset.

For each gene, we computed a 95% confidence interval (CI) for each estimated parameter using 200 non-parametric bootstraps with replacement of the samples. In human dataset, we generated new samples using a resampling of the participants within each experiment (i.e., FD and CR). In mouse, as each data-point was independent, new samples were generated by resampling each time-point independently, therefore keeping the same amount of data-point per time-points. With this method, we could ensure that new samples generated in mouse and human contain the same number of data-points and time-point coverage as the original data.

Dependance between parameters was assessed by computing correlations for each gene using bootstraps results. The parameters  $\beta_w$  and  $\beta_s$  were found to be negatively correlated (mean Spearman's correlation:  $\rho=-0.84$ ), because they were optimized for opposite sign and bigger differences increases the sleep-wake response amplitude.  $\gamma$  and  $\omega_0$  were found to be slightly positively correlated ( $\rho=0.38$ ). This correlation was driven by overdamped genes ( $\rho=0.56$ ; see example for cortical transcripts in Figure S7) and not observed ( $\rho=0.003$ ) for strongly underdamped genes ( $\zeta < 0.1$ ). Other optimized parameter pairs did not correlate.

### Model Comparisons

The full oscillator model ( $H_1$ ) was compared to 4 alternative models ( $H_A$ ) to explain expression dynamics. The first model ('Independent time-point effect') explains a gene expression ( $y$ ) as a multiple linear regression with an intercept and a vector of fixed effect ( $\beta$ ) for time-points ( $j$ ). Time-points are encoded as dummy variables matrix ( $X_j$ ). In mouse, this model has 18 parameters and 35 in human. 1 parameter per time-point + intercept; in human an extra effect is considered for the difference between the CR and FD experiments ( $\beta_{CR}$ )

$$y = \beta_0 + \beta_{CR} + \beta_j X_j + \epsilon$$

The 'Sleep-wake oscillator' model considers that sleep and wake are the only drivers of gene expression. The circadian drive is set to 0:

$$f_C = A \sin(\omega t + \varphi) = 0$$

This model therefore has 4 parameters in mouse:  $\gamma, \omega_0, \beta_w, \beta_s$  and 5 in human considering differences between FD and CR ( $\beta_{CR}$ ). The 'Circadian oscillator' model considers that the circadian drive is the only driver of gene expression. The sleep-wake drive is set to 0:

$$f_{sw}(t) = \beta_w W(t) + \beta_s S(t) = 0$$

This model therefore has 4 parameters in mouse:  $\gamma, \omega_0, A$ , and  $\varphi$ . And 5 in human, considering differences between FD and CR ( $\beta_{CR}$ ). The last model ('Circadian with sleep-wake masking') is a multiple regression model. Gene expression ( $y_i$ ) is described using a cosine model with a linear effect of sleep and wake amount at sampling time ( $t$ ). This model has 5 parameters in the mouse and 6 in human:

$$y = \beta_0 + \beta_{CR} + \beta_1 \sin(\omega t) + \beta_2 \cos(\omega t) + \beta_w W(t) + \beta_s S(t) + \epsilon$$

The null model ( $H_0$ ) is a simple linear regression with only an intercept:

$$y = \beta_0 + \beta_{CR} + \epsilon$$

We compared the BIC statistic of each of the 4  $H_A$  models and the  $H_0$  model to that of  $H_1$ . The BIC considers the model's goodness of fit while penalizing for complexity. A  $\Delta\text{BIC}$  was calculated for each of the 5 comparisons with positive values indicating support for  $H_1$  and negative values indicating support for  $H_A$  or  $H_0$ . A  $\Delta\text{BIC} > 2$  is considered as positive (2–6), strong (6–10), or very strong (>10) evidence.<sup>61</sup>

### PCA analysis

PCA analysis in mouse and human and projection of model fitted values were performed using R package FactoMineR.<sup>62</sup> Only transcripts with a  $\Delta\text{BIC}_{10} > 2$  were retained. Data matrix used for PCA analysis are composed of transcripts normalized expression (scaled  $\log_2$  CPM and  $\log_2$  intensities) for each time-points (i.e. 7237 [number of genes] x 62 [number of samples] in mouse cortex, 5770x62 in mouse liver, 18548x218 in human FD, 18548x427 in human CR). In human, 23.9% of transcripts contains at least 1 missing value (e.g. 98.7% of transcripts with < 3/218 missing expression in FD). Missing values were imputed using Rpackage missMDA. The ellipses were computed using 95% confidence interval of time-points barycentre. In human, missing values were imputed using R package missMDA.<sup>63</sup>

### Cortex and liver transcriptome timing

To estimate local biological time from clock genes in mouse cortex and liver, we used the R package TimeSignatR (<https://github.com/braunr/TimeSignatR>).<sup>48</sup> Baseline gene expression was used to train the elastic net, penalty parameter alpha and lambda were chosen using a leave-one-out cross validation. Predicted values were obtained from gene expression after sleep deprivation and from model fitted expression.

Using a similar strategy, local biological time was estimated for all rhythmic genes. We used the fitted expression level and fitted expression rate from our oscillator model as the 2 explanatory variables required to linearize circular time. Expression level and expression rate at ZT0, -6, -12, and -18 in baseline were fitted to the cartesian coordinate angle of a 24h clock using a bivariate linear model.<sup>48</sup> Genes were filtered for a minimal  $R^2$  value of 0.6 because rhythmic genes for which the baseline time course deviated too much from a sinewave-like dynamic scattered too much precluding reliable mapping to a 24h clock. 9 and 4% of all rhythmic genes were excluded in cortex and liver, respectively. Based on the fitted expression level and expression rate of our model after sleep deprivation, we predicted the corresponding time in baseline.